TUMOR GROWTH INDUCES OXIDATIVE CLUSTERED DNA LESIONS DAMAGE IN DISTANT MOUSE TISSUES *IN VIVO*

by Thomas Kryston

November 2010

Chair: Dr. Jeff McKinnon

Major Department: Biology

Our goal was to ascertain if DNA damage induced by oxidative stress is capable of being exploited as a precancerous or cancer biomarker. The specific DNA damage that we assessed was oxidatively induced non-DSB clustered DNA lesions (OCDLs). We further wanted to investigate if OCDL formation could be decreased by reducing reactive oxygen species (ROS) and oxidative stress. To accomplish this, we utilized the superoxide dismutase antioxidant, Tempol. Finally, we wanted to assess the role of specific cytokines and their part of inducing OCDLs in tissues both proximal and distal to a tumor mass.

For our first experiment, lung carcinoma cells were injected into nude mice in collaboration with the National Cancer Institute. We evaluated the DNA damage in various tisue samples, distal and proximal to the tumor, and compared the level the damage to control B6 mice with normal immune system. To conclude if reducing ROS effects OCDL accumulation, a cohort of NUDE mice were fed the antioxidant Tempol. To establish the effects of a fully functioning immune system on OCDL formation, tumor cells were also injected into a cohort of normal B6 mice.

The second experiment was performed to evaluate the specific roles that cytokines and inflammation play in inducing OCDL damage in tissues from tumor bearing mice. A cytokine analysis was previously performed by Redon *et al.* which indicated in the presence of Sarcoma,

monocyte chemoattractant protein-1 (MCP-1) was up regulated. To implement the specific role of MCP-1 in mediating the "bystander effect", our experiment entailed MCP-1 being knocked out for a group of mice and assessing the amount of OCDL damage in various tissues.

We utilized repair enzymes as probes to measure the level of OCDLs. These repair enzymes, human APE1, human OGG1, and *E. coli* Endo III, have functional activity in vivo. Once detection of a lesion in a cluster occurs, excision of the damaged base and of the DNA strand will transpire. Each DNA strand will now display a single stranded break which, if within 1-10 base pairs, results into a double stranded break. These additional breaks are measured as clustered lesions and assessed via neutral agarose gel electrophoresis and calculated with number average length analysis (NALA).

Earlier prognosis and detection of a growing tumor is a significant aspect of successful treatment. From these experiments, we hope to establish OCDLs as precancerous or cancer biomarkers in the case of high oxidative stress. It is hopeful one day clinical biopsies can be performed to screen for this specific damage and indicate early complications and tumor growth.

Future experiments can be projected based on our study. Different tumors can be utilized to assess OCDL damage. An inclusion of wider variety of tissues will further establish the complex DNA damage induced by the bystander/distal effect with ROS and inflammation as mediators of this damage.

TUMOR GROWTH INDUCES OXIDATIVE CLUSTERED DNA LESIONS DAMAGE IN DISTANT MOUSE TISSUES *IN VIVO*

A Thesis Presented To The Faculty of

The Department of Biology

East Carolina University

In Partial Fulfillment of the

Requirements for the Degree

Master of Science in Molecular Biology and Biotechnology

By Thomas Kryston

November, 2010

TUMOR GROWTH INDUCES OXIDATIVE CLUSTERED DNA LESIONS DAMAGE IN DISTANT MOUSE TISSUES *IN VIVO*

TUMOR GROWTH INDUCES OXIDATIVE CLUSTERED DNA LESIONS DAMAGE IN DISTANT MOUSE TISSUE *IN VIVO*

by

THOMAS KRYSTON

APPROVED BY:

DIRECTOR OF THESIS: _____

Dr. Alexandros Georgakilas, Ph.D

COMMITTEE MEMBER: _____

Dr. Michael Dingfelder, Ph.D.

COMMITTEE MEMBER: _____

Dr. Thomas McConnell, Ph.D.

COMMITTEE MEMBER: _____

Dr. Baohong Zhang, Ph.D.

CHAIR OF THE DEPARTMENT OF BIOLOGY: _____

Dr. Jeff McKinnon, Ph.D.

DEAN OF THE GRADUATE SCHOOL: _____

Dr. Paul J. Gemperline, Ph.D.

ACKNOWLEDGEMENTS

I am thankful for the opportunity that Dr. Alexandros Georgakilas has provided me to work in his laboratory. His guidance and support throughout the course of my thesis work has truly inspired me. I would also like to thank Dr. Michael Dingfelder, Dr. Thomas McConnell and Dr. Baohong Zhang for their indispensable advice and comments provided towards my project.

I would also like to express my appreciation to fellow lab members, Khaled Aziz, Anastassiya Georgiev, Nicholas Ferguson, Thomas Santangelo, and others for their assistance provided towards the completion of this project.

I would also like to thank the loving support I have received from my wife, Brittany Kryston, friends and family.

Funding for this project was provided to Dr. Georgakilas by the Department of Biology at East Carolina University, a Research and Creativity Grant and a College Research Award. I would also like to sincerely thank Dr. William Bonner and Dr. Olga Sedelnikova for providing the tissues for the experiments and performing all the *in vivo* work.

TABLE OF CONTENTS

LIST OF TABLES

LIST OF FIGURES

LIST OF ABBREVIATIONS

APE1	Apurinic / Apyrimidinic Endonuclease 1
AP	Apurinic / Apyrimidinic site
ATP	Adenosine Triphosphate
B6	Normal mice
bp	Base pair
BER	Base Excision Repair
CCL-2	Chemokine (C-C) Ligand 2
DMSO	Dimethyl sulfoxide
DNA	Deoxyribonucleic acid
DSB	Double strand break
DTT	Dithiothreitol
EDTA	Ethylene Diamine Tetraacetic Acid
Endo III	Endonuclease III
Gbp	Giga Base pairs
GI	Gastrointestinal
H2AX	Histone H2AX
hAPE1	Human Apurinic/ Apyrimidinic Endonuclease 1
HCl	Hydrochloric Acid
hOGG1	Human 8-oxoguanine DNA glycosylase
IC	Inflammation Control
IR	Ionizing Radiation
Kbp	Kilo Base pairs

KO	Knocked Out
MAP	Mouse Antibody Production
MCP-1	Monocyte Chemoattractant Protein-1
$MgCl_2$	Magnesium Chloride
mM	Milli Molar
M	Molar
Mbp	Mega Basa Pairs
NaCl	Sodium Chloride
NADPH	Nicotinamide Adenine Dinucleotide Phosphate Hydrogenase
NALA	Number Average Length Analysis
NER	Nucleotide Excision Repair
NC	Normal Control
NCI	National Cancer Institute
NIH	National Institute of Health
NSS	Native Stop Solution
Nt	Nucleotide
OCDL	Oxidatively Induced Clustered DNA Lesion
PBN	N-tert-butyl-alpha phenyl nitrone
PBS	Phosphate Buffered Saline
PCR	Polymerase Chain Reaction
PKC	Protein Kinase C
RNS	Reactive Nitrogen Species
ROS	Reactive Oxygen Species

SSB	Single Strand Break
TBE	Tris Borate Ethylene Diamine Tetraacetic Acid
TE	Tris Ethylene Diamine Tetraacetic Acid
Tg	Thymine Glycol
TGF-β	Transforming Growth Factor- β
TST	Test mouse with tumor
UV	Ultraviolet
XRCC1	X-ray repair complementing defective repair in Chinese hamster cells 1

CHAPTER 1: INTRODUCTION

In 2010, the projected second leading cause of death is cancer (CDC, 2010). This being so, it is imperative more knowledge about the disease and mechanisms be understood. With further investment, earlier detection can be achieved, ultimately leading to better prognosis.

Damage to DNA occurs frequently and varies in type and complexity. It can range from simple single strand breaks, double strand breaks, and base damages to more complex closely spaced lesions i.e. clustered DNA damage (FIGURE 1). All these damages are characteristically repaired via conventional repair mechanisms for instance through base excision repair (BER) (FIGURE 2), nucleotide excision repair (NER), and double stranded break (DSB) repair. Inaccurate and insufficient repair of this impairment can often lead to mutations, genomic instability, transformation and formation of cancer.

Radiolytic attacks to DNA that lead to damage can be divided into two broad categories based on the source: endogenous and exogenous. Exogenous attacks arise from specific interaction to ionizing radiation such as X-,γ-, or cosmic rays. Endogenous attacks originate from natural occurrences inside the body for instance through cell signaling, metabolic processes and inflammation (Vilenchik and Knudson, 2003). During endogenous attacks, the primary source of damage to DNA is attributable to reactive oxygen species (ROS) and reactive nitrogen species (RNS). Formation of ROS/RNS occurs throughout the body. In the mitochondria, ROS is formed as a byproduct during oxidative phosphorylation. In macrophages and neutrophils, ROS is synthesized enzymatically. ROS has the capability to react with proteins, lipids, and DNA, leading to damage. Abasic sites, oxypyrimidines, oxypurines, single stranded breaks (SSB) and double stranded breaks (DSB) are the typical types of damage associated with ROS's interaction with DNA.

Improper repair and accumulation of the associated damages may lead to mutations, various pathophysiological conditions like “aging”, and potentially cancer. Based upon the complexity of the damage, different repair systems are implemented ultimately leading to different outcomes (FIGURE 3). Base Excision repair is a repair system that utilizes several different enzymes. OGG1 is an enzyme that recognizes oxypurines and hydrolytically cleaves and eradicates the damaged base via N-glycosylase activity. This creates an apurinic (AP) site. The AP-lyase activity creates an incision 3’ to the sugar which has the missing base. Polymerase β inserts the missing base, followed by DNA ligase III sealing the gap (Georgakilas, 2008).

Endonuclease III (ENDO III) is a glycosylase that acts in a similar fashion. ENDO III acts, upon other substrates, on oxypyrimidines. Upon recognition of the oxypyrimic site, N-glycoslyase activity releases the damage pyrimidine. The AP-lyase activity cleaves the phosphdiester bond 3’ to the AP site leaving a 5’ phosphate and a 3’ ring opened sugar (Gros, et al. 2002; Georgakilas, 2008).

Human apurinic/apyrimidinic (AP) endonuclease (APE1) is a damage probe that cleaves the DNA backbone immediately 5’ to the AP site, generating a single-strand break, leaving a 3’ –hydroxyl and 5’ –deoxyribose phosphate terminus (Georgakilas, 2008).

Simple DNA lesions utilize this repair and enzymes with superior efficiency. When the DNA damage is more complex, repair efficiency decreases. When two or more lesions occur within 1-10bp, the damage is said to be clustered. If these clusters are induced by oxidative sources, they are more properly known as oxidatively induced clustered DNA lesions (OCDL) (Sutherland et al. 2000). OCDLs have been demonstrated to create hindrances to normal efficient DNA repair processes. It was first introduced by Chaudry and Weinfeld that DNA lesions are repaired sequentially, meaning as the completion of repair to one lesion occurs, the initiation of

repair to the next takes place (Chaudry and Weinfeld, 1997). With clustered DNA lesions, it has been suggested that due to the close vicinity, DSBs can occur (Georgakilas, 2007).

In vivo verification of OCDLs damage being repair resistant was seen from a study performed by Gollapalle *et al.* in 2007. Mice were exposed to exogenous radiation and displayed increased levels of OCDL damage 20 weeks after initial exposure. Interestingly, it was seen that distal tissues, which were protected from the radiation, too showed increased levels of OCDLs. The mechanisms behind this effect, known as the bystander/distal effect, are still not completely understood. Little *et* al, demonstrated that suppression of the bystander effect can be seen with the addition of a superoxide dismutase and inhibition of NADPH oxidase, indicating oxidative stress as the mediator to this effect (Little and Azzam, 2002). Further studies have implicated this effect to be arbitrated by several factors associated with oxidative stress, including inflammation, cytokines, and cellular signaling (Redon et al. 2010*).* To attempt to address which cytokine(s) may play a role in the bystander/distal effect *in vivo*, Redon e*t al.* performed a cytokine analysis. One cytokine found in elevated levels in sarcoma bearing mice was the monocyte chemoattractant protein 1 (MCP-1) also known as chemokine (C-C) ligand 2 (CCL-2).

Inflammation is an essential mechanism in our body during immune responses. Cells of the immune system, such as macrophages and neutrophils, function by releasing chemicals or cytokines that disrupt foreign membranes, increase opsonization, provide chemotaxis, and elevate inflammation (Sebald and Nikel, 2009). The cytokine monocyte chemoattractant protein-1 (MCP-1) was first illustrated to function as a necessary signal for recruitment of monocytes to a site of injury where differentiation can occur to macrophages. Since, MCP-1 has been implicated as a source for numerous inflammatory diseases (Brewald et al, 2007; Dewald et al, 2005; Popivanova et al, 2009). MCP-1 also functions as a stimulant to the production of

transforming growth factor β (TGF-β). TGF-β is a protein that is normally found in the body that regulates cell growth by inhibition. Cancerous cell's TGF-β pathway display mutations and was seen, when added to cell cultures at increased levels, induced DNA lesions (Sokolov et al, 2005; Sedelnikova et al, 2007; Prise and O'Sullivan, 2009).

To attempt to utilize OCDLs and phosphorylated histone H2AX as cancer biomarkers, especially in the case of oxidative-stress related cancers, Redon *et al* designed a study comparing the frequency of the associated damage in different tissues in tumor bearing mice. The tissue samples were as follows: duodenum, colon, rectum, stomach, liver, kidney, lungs, ovary, skin, bone marrow, and spleen. The associated tumor was melanoma or adenocarcinoma. Redon *et al* examined levels of phosphorylated histone H2AX (γ-H2AX), which indicates the presence of DSBs (a form of clustered DNA lesions). DNA lesions were indeed shown at elevated levels. Tissues that replicate frequently displayed further elevation of DSBs and OCDLs and greater sensitivity to the bystander/distal effect.

To further this study, we modified the protocol and executed an additional set of experiments. For the first experiment, we had six sets of mice, six mice per set, and six different cohorts. Six mice were PBS sham controls. To address the role of inflammation with respect to OCDL formation, six mice were fed with Freund's adjuvant as an inflammation control. To identify the potential increase in oxidative damage in association with the presence of tumors, six nude mice were injected subcutaneously with lung carcinoma cells. Six lung carcinoma bearing nude mice were fed the antioxidant Tempol (FIGURE 4) to elucidate the effects of antioxidants in the presence of tumors. A corresponding set of mice were fed Tempol to identify a base level as a control. To test the possible role of the immune system in the accumulation of OCDLs, a final set of six B6 lung carcinoma bearing normal mice were added. We hypothesized a growing

lung carcinoma tumor will induce a higher amount of OCDLs than in control mice tissues (distant and proximal to the tumor). Also, with the presence of lung carcinoma, the tissues that are most proximal to the carcinoma will display the highest amounts of OCDLs compare to distant.

Tempol, 4-hydroxy-2,2,6,6-tetramethylpiperidine-1-oxyl, is a nitroxyl radical, with membrane permeable properties. It acts as a superoxide dismutase mimetic that seeks and neutralizes superoxide anions (Chatterjee, 2000).

In order to assist with the determination if the absence of MCP-1 abrogates DNA damage in tumor bearing mice, a second experiment was performed. Two different groups were established, four sets, five mice per set per group. The first group, MCP-1 was knocked out. One set of mice were injected subcutaneously with sarcoma cells. A second set of mice were injected subcutaneously with melanoma cells. To maintain a background level of oxidative damage, a control of five mice were utilized. To establish again an inflammation control, five mice were fed Freund's adjuvant. Two tissues were analyzed: duodenum and colon.

The second group for this experiment maintained the same cohorts, but utilized normal B6 mice as opposed to MCP-1 ko. We hypothesized the mechanism involved in OCDL induction in tumor bearing mice involves MCP-1 cytokine and use of antioxidant tempol will reduce the OCDL levels, verifying the presence of high oxidative stress in animals.

Figure 1: Simple vs. Complex DNA Damage

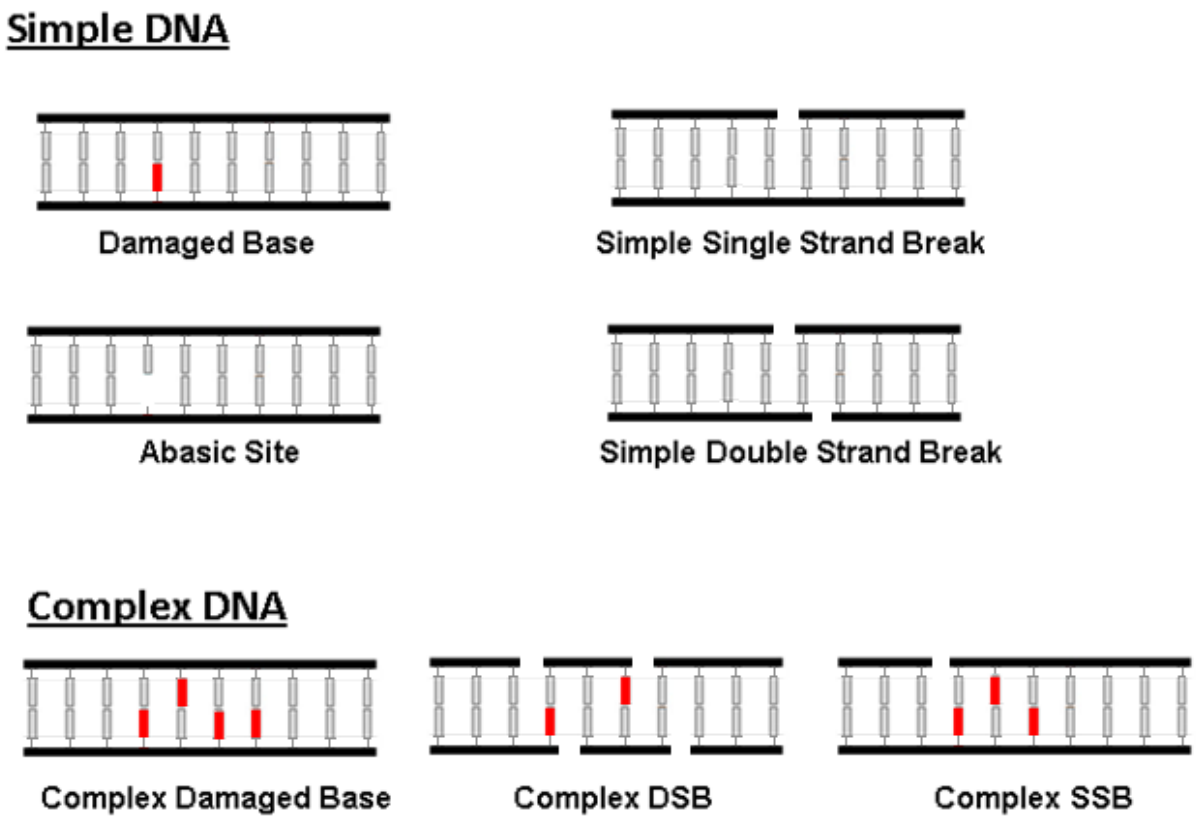

Figure 1: Simple DNA damage is illustrated above. Single lesions exhibit exceptional proficiency in repair. Clustered DNA damage is defined as two or more damaged bases or lesions present in opposing strands within 1 to 10 base pairs. Clustered DNA lesions have been demonstrated to be repair resistant. Light squares denote undamaged bases. Damage to individual nucleotides comprise missing or damaged (red squares) bases and strand breaks (accompanied by base loss).

Figure 2: Base Excision Repair Pathway

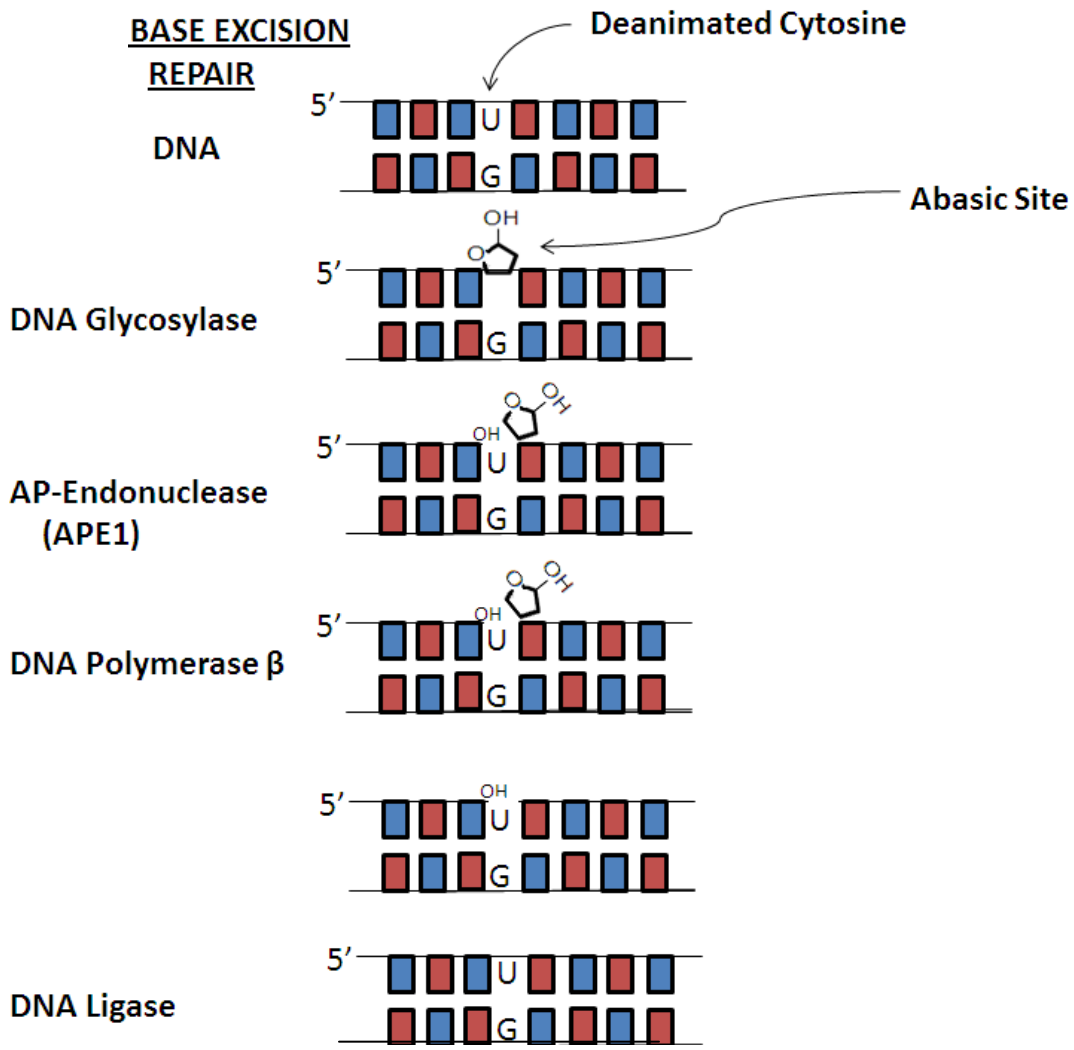

Figure 2: Several enzymes are utilized during base excision repair (BER). Specific enzymes can recognize and hydrolytically cleave and eliminate the impaired base, creating an apurinic/apyrimidinic (AP) site. This AP site is acted on APE1 which creates an incision 5` to the sugar which was missing the base. DNA polymerase β inserts the missing base, followed by the patching of the single nucleotide gap. The final player is DNA ligase III and XRCC1 complex which seals the gap.

Figure 3: ROS Effects on DNA

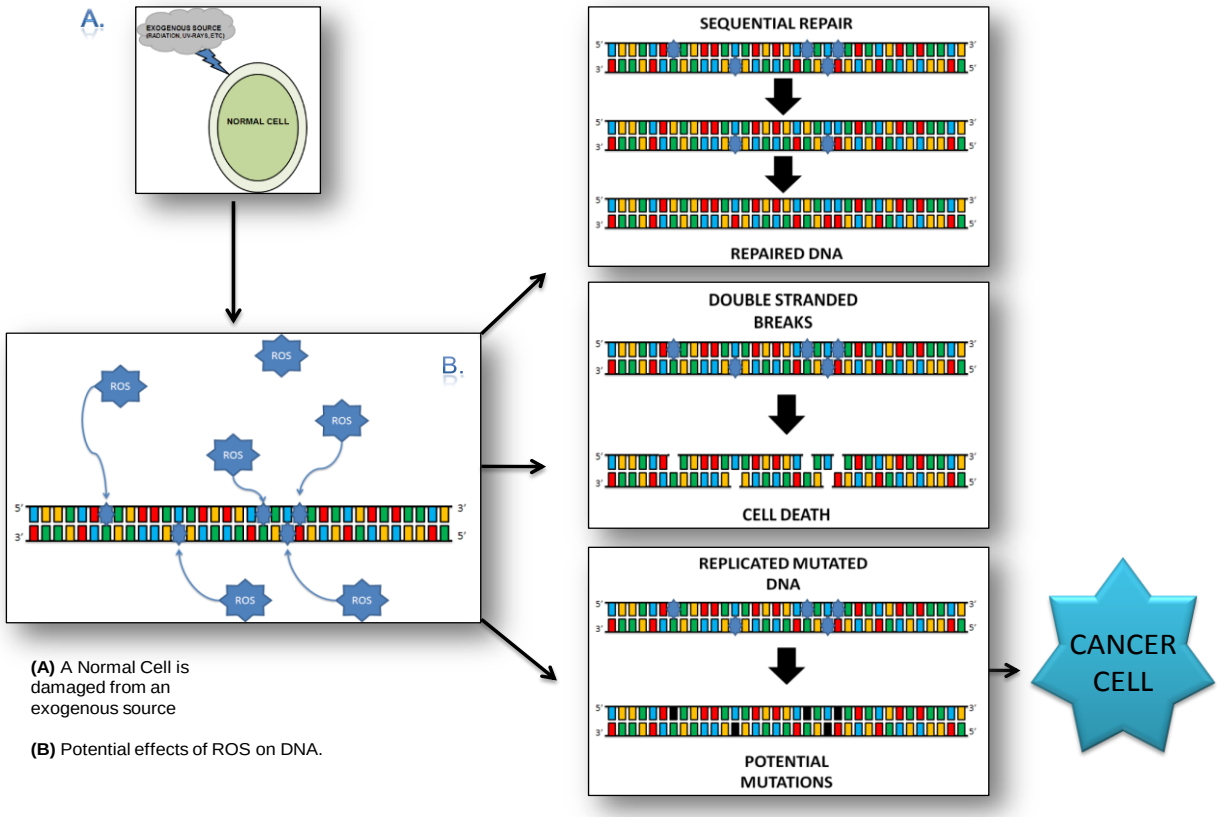

Figure 3: Potential formation of ROS. In 3A, a mutation is introduced by an exogenous source. Figure 3B exemplifies the outcome of the newly created ROS and its interaction with DNA. Three outcomes from this interaction are displayed. In one scenario, the DNA will utilize sequential repair through the use of the primary repair systems NER and BER. The DNA is then repaired successfully. The second scenario is shown where no repair occurs leading to DSB and ultimately cell death. The final scenario depicts mutations generated from the improper repair. Cells with the mutations replicate, potentially leading to the creation of cancer cells.

Figure 4: Structure of Tempol

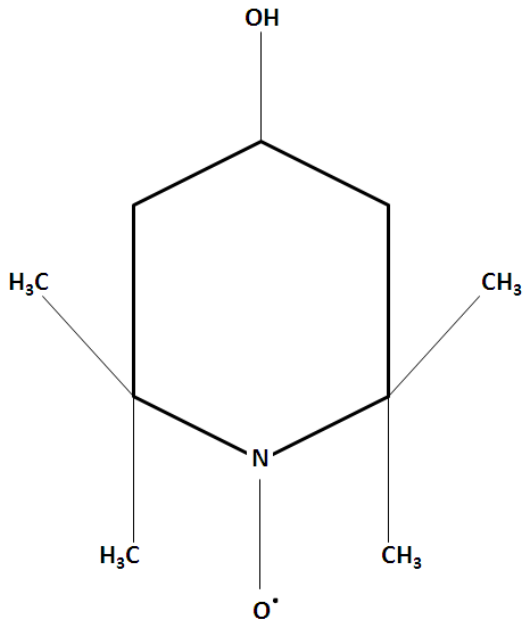

Figure 4: Antioxidant utilized in the Lung Carcinoma Experiment. 4-hydroxy-2,2,6,6-tetramethylpiperidine-1-oxyl. Tempol characteristics are: Water soluble, low MW, permeates biological membranes, scavenges superoxide anions in vitro, superoxide dismutase mimetic, reduces intracellular concentration of Fe^{2}+, and hence the formation of hydroxyl radicals via Fenton or Haber- Weiss reaction, short half life, and can switch between oxidized/reduced forms.

CHAPTER 2: OBJECTIVES

The first experiment determined the effects lung carcinoma has on the formation of OCDLs in different organs. Six sets, six mice per set were utilized. The first set of six mice were normal control. A second set of mice were injected with Freund's adjuvant. This adjuvant stimulated inflammation, allowing us to determine the role of basal inflammation plays in damage associated with an increase in oxidative stress. It is hypothesized inflammation is a contributable factor in the bystander effect. This adjuvant allowed us to assess the DNA damage with regards to this effect. A third set of six mice were nude mice injected with lung carcinoma cells. Nude mice lack a thymus. Without the thymus, no T-cell mediated immune response can occur. With implementing nude mice in the experiment, we could determine the level of DNA damage from specific sources. We compared the number of OCDLs in tissue DNA samples from these tumor bearing mice to the inflammation control mice. A set of nude lung carcinoma bearing mice were fed the antioxidant Tempol. By doing so, determination of the inhibition of ROS decreasing OCDL accumulation was made. A corresponding set of control plus the antioxidant Tempol was utilized for this comparison. A set of B6 normal mice were induced with lung carcinoma to determine the effect(s) of the immune system. The organs that were assessed were: Ovary, Lung, Spleen, Duodenum, Stomach, Colon, Rectum, Skin Distal to tumor, Skin Cervical to tumor, and Tumor Mass.

A second experiment was performed to investigate the role of MCP-1 in the induction of OCDL damage. To execute this experiment, the gene encoding MCP-1 was knocked out. Four sets, five mice per set were utilized. One set of mice were the MCP-1 knocked out (ko) control. A set of mice were injected with Freund's adjuvant for an inflammation control. A third set of MCP-1 ko mice were inject with sarcoma cells. A final set of MCP-1 ko mice were injected with

melanoma cells. The duodenum and colon were the tissues analyzed for OCDL damage. To establish the effects sarcoma and melanoma obtain, the experiment was replicated using normal B6 mice.

To compare the levels of OCDL damage, three repair enzyme probes were utilized: APE1, OGG1, and EndoIII. These enzymes function, *in vitro*, by detecting damaged DNA damage (TABLE 1). As a lesion is detected, the enzyme excises the damaged base and cleaves the DNA strand. From this, a single stranded break in each strand ensues. This in turn forms a double strand break, when within 0-20 bp, which is measured through an adaptation of non-denaturing agarose gel electrophoresis and number average length analysis (NALA).

Table 1: Repair Enzymes

Repair enzyme used as damage probe	Substrates
Human APE1 or *E. coli* Nfo protein (Endonuclease IV)	Abasic: Several types of abasic sites including oxidized abasic sites, abasic sites modified with alkoxyamines and DNA containing urea residues.
Human OGG1 or *E.coli* Fpg protein (DNA glycosylase) Associated AP lyase activity	Oxypurines: Oxidized purines, FapyGua, FapyAde, C8-oxoGuanine, some abasic sites, C8-oxoAdenine and to a lesser extent, other modified purines.
Human NTH1 protein or *E.coli* EndoIII (Endonuclease III) Associated AP lyase activity	Oxypyrimidines: Thymine residues damaged by ring saturation, fragmentation, or ring contraction including thymine glycol (Tg) and uracil residues (5-fo-Ura), FapyAde, 5-OH-Cyt and to a lesser extent FapyGua.

Table 1: Repair enzymes that were utilized in our experiments and their corresponding DNA damage substrates.

Figure 5: Overview of Lung Carcinoma Experiment

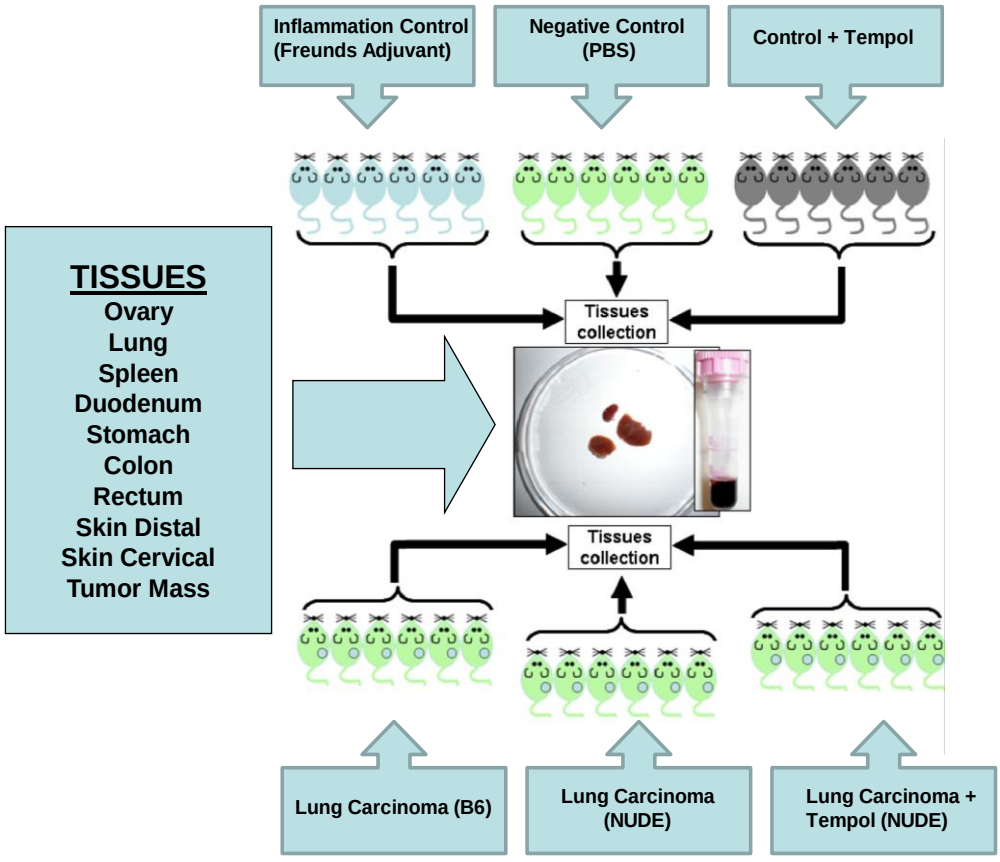

Figure 5: This is a schematic of the Lung Carcinoma experiment, showing the different sets of treatment. Five sets of nude mice were utilized: normal control with no treatment, inflammation control injected with Freund's adjuvant, antioxidant treated control, lung carcinoma bearing, and lung carcinoma bearing fed the antioxidant Tempol. A set of B6 mice were also injected with lung carcinoma cells to determine the effect of the normal immune system on OCDL damage.

Figure 6: Overview of MCP-1 ko and B6 Experiment

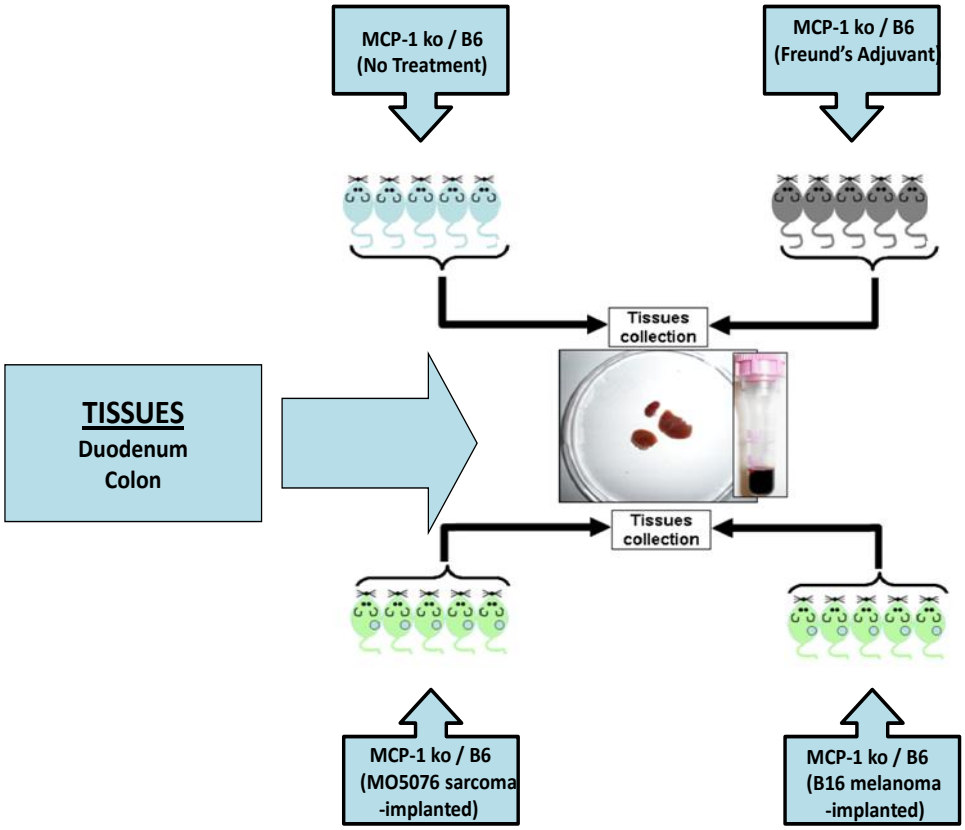

Figure 6: This is a schematic of the MCP-1 ko and B6 (normal immune). Two groups were utilized. The first group had the gene encoding MCP-1 knocked out. There was four sets, each set containing five MCP-1 ko. The first set of MCP-1 ko mice were normal control with no treatment. Second, an inflammation control injected with Freund's Adjuvant. Two tumors were tested: sarcoma and melanoma. The same format was followed but with normal B6 mice. This provided a control to the MCP-1 ko experiments.

Figure 7: Agarose gel showing Clustered DNA Damage (Example)

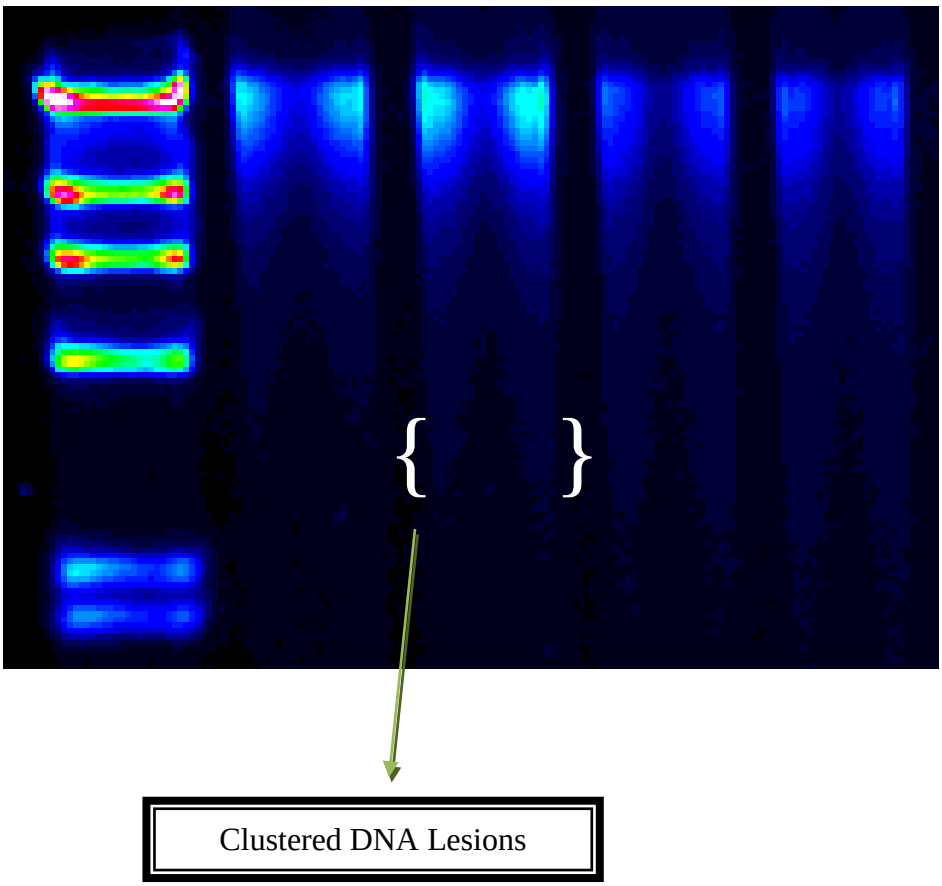

Figure 7: From left -

Lane 1: DNA λ-HIND III digest (utilized as marker)

Lane 2: DNA No enzyme

Lane 3: DNA Enzyme treated

Lane 4: DNA No enzyme

Lane 5: DNA Enzyme treated

CHAPTER 3: HYPOTHESIS

We have three hypotheses:

1. Growing lung carcinoma will induce a higher amount of OCDLs in tumor bearing mice compared to normal mice tissue (distant and proximal to the tumor).

2. With the presence of lung carcinoma, the tissues that are most proximal to the carcinoma will display the highest amounts of OCDLs compared to distant.

3. The mechanism involved in OCDL induction in tumor bearing mice involces MCP-1 cytokine and use of antioxidant Tempol will reduce the OCDL levels, verifying the presence of high oxidative stress in animals.

CHAPTER 4: METHODS

Tissue Source

The mouse DNA samples were a gift from Dr. Sedelnikova and Dr. Bonner from Center for Cancer Research, NIH. The lung carcinoma experiment utilized expansively characterized, MAP tested, and cryoarchived samples of mouse Lewis (NSC-224131) lung carcinoma (host strain C57BL/6). These were obtained from the DCTD tumor repository at NCI-Frederick. The lung carcinoma was first passaged through "donor" mice. After, it was implanted into 6 test nude mice; 6 mice were subjected to a single subcutaneous injection of complete Freund's adjuvant, and other 6 mice served as a sham control. After two weeks, all animals were sacrificed followed by DNA damage assessment on various tissues.

To investigate the mechanisms of the bystander/distal effect and associated DNA damage from possible elevation of oxidative stress from the presence of a tumor, an additional cohort was introduced. Six tumor-bearing mice were fed Tempol, an antioxidant. A corresponding control group of mice were fed Tempol with no tumor treatment. Both cohorts followed the protocol as described above. The antioxidant Tempol was obtained from Dr. James Mitchell, Radiation Biology, NCI. The Tempol was administered as 10 mg Tempol/gram of chow. To adjust accordingly for the diet, mice were fed the antioxidant two weeks prior to the experiment and continued the two weeks of the experiment. Body weights were taken at the feeding start point, the first day of experiment, and at the time of sacrifice.

To examine the role of cytokines in mitigating the increase in oxidative damage, ten B6 and ten MCP-1 ko normal mice were implanted with melanoma and sarcoma cells. The procedures were replicated as described above.

Isolation of DNA

The "High Pure PCR Template Kit" (Roche, Indianapolis, IN) was utilized for isolating DNA from the mouse tissues. As stated from the manufacturer, DNA fragments yielded ranged from six to 28kbp. Tissues were stored at -20°C until isolation was performed. Once removed, tissues were kept on ice. Samples were incised into smaller fragments to improve nucleic acid amount yielded. 25-50mg of tissue sample was obtained. In a nuclease-free 1.5 mL micro centrifuge tube, 200µl of tissue lysis buffer (4M urea, 200mM Tris, 20mM NaCl, 200mM EDTA, pH 7.4) was added followed by 40µl of reconstituted Proteinase K. Proteinase K was added to assist with the inactivation and degradation of endogenous DNase and sample lysis. The sample was mixed immediately and placed in an incubator for 12 hours at 37°C. Once 12 hours were complete, 200µl of binding buffer was added followed by being vortexed. The sample was then placed in an incubator for 10 minutes at 65°C. After 10 minutes, 100µl of isopropanol alcohol was added and vortexed. Any insoluble tissue segments were removed using a 1000µl sterile pipette tip. The sample material that remained in the microcentrifuge tube was then transferred into a High Filter tube located inside a Collection tube. 500µl of Inhibitor Removal Buffer (5M guanindine-HCl, 20mM Tris-HCl, 37.7% absolute ethanol (v/v), pH 6.6) was added. The microcentrifuge tube and Collection tube was then placed in a centrifuge and spun for one minute at 8,000g. The Collection tube was then discarded. The High Filter tube, containing the sample, was removed and placed into a new Collection tube. 500µl of wash buffer (80% absolute ethanol (v/v), 20mM NaCl, 2mM Tris-HCl, pH 7.5) was added to the High Filter tube and spun down at 8,000g for one minute. The wash was repeated twice. The Collection tube was discarded and the High Filter tube was placed in a new, sterile collection tube. The tubes were again placed in a centrifuge and were spun down at 14,000g for 15 seconds. To elute the DNA, the High Filter

tube was placed into a sterile 1.5 mL microcentrifuge tube. 200µl of pre-warmed (65°C) Elution Buffer (10mM Tris-HCl, pH 8.5) was added to the assembly and centrifuged for 75 seconds at 8,000g. Upon completion, the 1.5 mL microcentrifuge tube contained the isolated DNA from the sample.

Measurement of DNA concentration

1µl of the DNA sample was analyzed using a nanodrop spectrophotometer. This calculated the amount of sample required for analysis of the DNA. The Absorbance readings were read at 260nm and 280nm automatically. To blank the nanodrop, 1µl of TE buffer (10mM Tris-HCl, 1mM EDTA, pH 7.5) was utilized as a control. The purity and concentration of the DNA sample was derived from these values.

Detection and measurement of oxidative clustered DNA lesions

To detect the OCDL levels (FIGURE 8), constant gel electrophoresis along with quantitative analysis and number average length analysis (NALA) was performed. Microcentrifuges tubes were utilized to contain the sample during analysis. 1 µl of DNA was added with 6.5 µl of the appropriate enzyme buffer was added into the microcentrifuge tube and left on ice. The buffers utilized were: APE1 buffer (50mM potassium acetate, 20mM Tris acetate, 10mM magnesium acetate, pH 7.9), OGG1 buffer (50mM NaCL, 10mM $MgCl_2$, 10mM Tris-HCl, pH 7.9), and EndoIII buffer (20mM Tris-HCl, 1mM EDTA, pH 8.0). Each sample was analyzed with no enzyme (negative) followed by with enzyme addition (positive). The repair enzymes APE1, OGG1, and ENDO III were used as the enzymatic probes and hydrolytically cleaved the DNA at their specific oxidative damaged site as summarized in (Table 1). Next was

the addition of 1µl of dithiothreitol (DTT, 10mM; Sigma). Samples were left to incubate for five minutes on ice. For the positive set, 1 µl of the appropriate was added (1 unit for hAPE1 and EndoIII, 0.2 units for hOGG1), followed by five seconds of vortexing. Samples were then transferred to 37^{o}C water bath and incubated for 65 minutes. After incubation, 5µl of ice cold Native Stop Solution (NSS) was added. The samples were then placed on ice for 60 minutes. After 60 minutes, samples were loaded onto gels (85% agarose (w/v); Biorad) and placed into the chamber filled with 0.25X TBE (22.25mM Tris-borate, 0.5mM EDTA) and left for 10 minutes to equilibrate. After equilibration, constant gel electrophoresis was performed and ran for three hours and 40 minutes at 50 V. Gels were then stained with Ethidium Bromide (1 ng/µl) and left overnight for de-staining. λ-HIND III digest (Fisher) was utilized as the DNA standard and also run on the gel. Preparation consisted of the addition of 5µl of TE buffer, 5µl of NSS, and 0.75µl of marker. It was then placed in 65^{o}C for three minutes and left on ice until the gel was ready for loading.

Electronic gel images were obtained through FluorChem 8900 imaging system and AlphaEase FC software (Alpha Innotech, San Leandro, CA). Samples were processed using Quantiscan software (Biosoft, Ferguson, MO) and a densitogram was obtained (FIGURE 9). The program Origin 6.1 (Origin Lab, Northampton, MA) was utilized to plot a dispersion curve (FIGURE 10) using the marker which acted as the DNA standard contained bands between two and 23.1kbp.

The frequency of various clusters were obtained using the contour length of DNA molecules migrating to a certain position and the fluorescence profile of a lane, which was outlined in the procedure by Sutherland *et al* (Sutherland, Bennett et al. 2003).

If a population of N_u duplex DNA molecules in which the i^{th} molecule contains L_i base pairs, the average length of the molecules in the population can be expressed by Equation {1}.

$$\bar{L}_U = \frac{\sum_{i=1}^{N} Li}{N_U} \qquad \{1\}$$

The sum in the numerator on the right side of Equation {1} is the number of base pairs present in the sample. The subscript "U" indicates that the sample is untreated. When a sample is treated with an enzyme, it introduces M double strand breaks in the N_u molecules in the population. These breaks could be randomly distributed, be produced at specific sites in the molecules, or have many other distributions. Regardless of the distribution, each strand breaks result in the formation of two smaller molecules. Consequently, the number of molecules in the population treated N_T can be represented by N_u + M molecules. The average length of the molecules in this population is shown in Equation {2} where "T" denotes a treated sample.

$$L_T = \frac{\sum_{i=1}^{Nu+M} Li}{N_U + M} \qquad \{2\}$$

With the formation of a single strand break, the number of molecules increases but the number of base pairs does not. Because of this, the sum in the numerators of Equation {1} and {2} are the same. Both can be substituted with N_{bp}, the number of base pairs in the population. Upon rearrangement of the equation $N_T=N_U$ + M we obtain $M=N_T-N_U$. Dividing by N_{bp} we can get the frequency of the breaks (Φ). This is shown in Equation {3}.

$$\phi = \frac{M}{N_{bp}} = \frac{N_T}{N_{bp}} - \frac{N_U}{N_{bp}} \qquad \{3\}$$

When we replace N_{bp} for the sums in Equations {1} and {2}, we obtain:

$\bar{L}_U = N_{bp}/N_U$ and $\bar{L}_T = N_{bp}/N_T$.

When we swap these expressions into Equation {3}, we get the expression for frequency as shown in Equation {4}.

$$\phi = \frac{1}{\bar{L}_T} - \frac{1}{\bar{L}_u} \qquad \{4\}$$

For molecules whose lengths are measured in base pairs, the (Φ) is the probability of a strand break per base pair. Thus (Φ) is the frequency of breaks induced by the treatment, and is determined in units such as breaks/Gbp by measurement of average length of molecules in a population before and after enzyme treatment. Since both the numerator and denominator of Equations {1} and {2} scale as the mass of DNA, not all of the molecules in that population need to be measured, but only a representative sample. The determination of average lengths is insensitive to the mass of sample chosen, as long as it is low enough so that individual molecules migrate as a function of their length (Sutherland *et al*. 2003).

A outline view of the procedure:

1. DNA isolated from tissue
2. Treated or not treated with repair enzyme
3. Constant field agarose gel elctrophoresis performed
4. Gel stained with Ethidium Bromide
5. Image obtained using FluoroChem 890 imaging system from Alpha Innotech.
6. Intensity profiles generated by Quantiscan software
7. Dispersion curve (size vs migration) prepared by using Origin 6.0 for the marker fragments.

a. Second order exponential fit yields equation with parameters (y0,a1,t1,a2,t2)

8. The contour length of the DNA molecules migrating to a certain position and the fluorescence profile of a lane is used to calculate the frequency of OCDLs.
    a. Area calculated using trapezoid rule
    b. Half point of migration (x_{med}) is found
    c. The standard curve and parameters from the marker fragments is utilized to convert the point of half migration (x_{med}) to the median length in bases (L_{med})
    d. The median length in bases (L_{med}) is converted to average molecular length (L_n)using the equation $L_n = 0.6\ L_{med}$
    e. Determine number of clusters (Φ) using the equation: $\Phi = 1/L_T - 1/L_U$
        i. Where, L_T= average molecular length of treated sample
        ii. L_U=average molecular length of untreated sample
        iii. Φ=number of clusters (bp)

        (Sutherland *et al*. 2003).
    f. Statistical analysis was performed using the student paired T-test; $p<0.05$.

Figure 8: Clustered DNA Damage Detection Using Repair Enzymes as Damage Probes

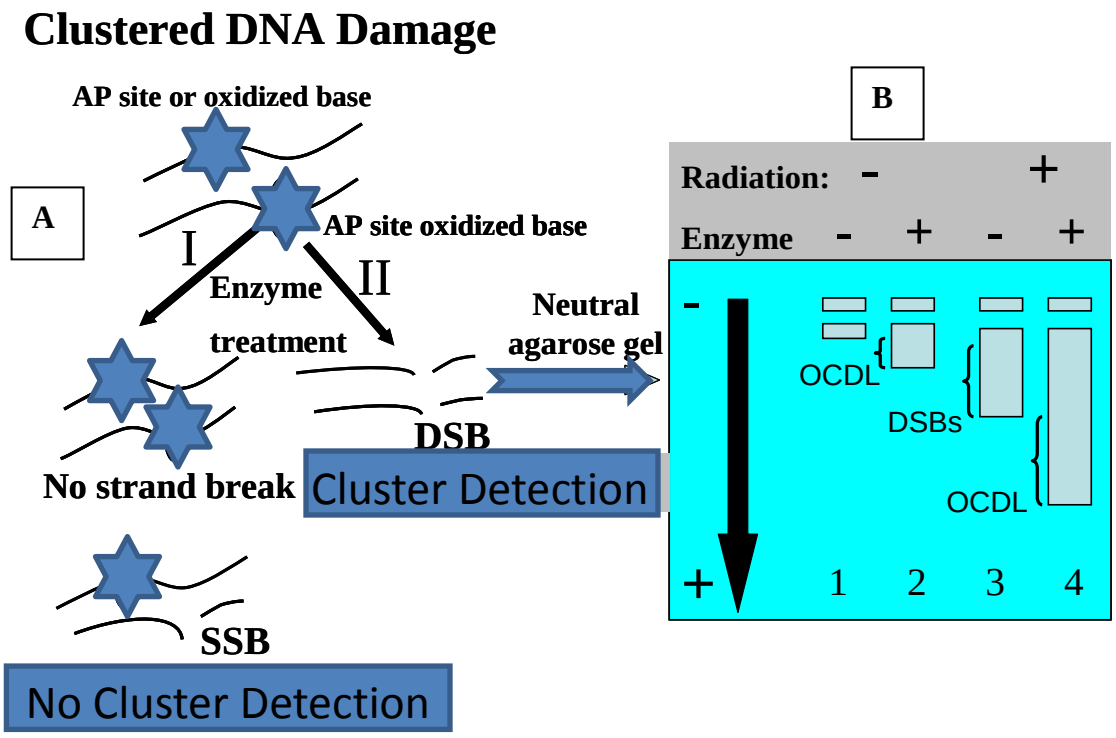

Figure 8: Detection of clustered DNA lesions (double strand breaks, DSBs and oxidative clustered DNA lesions, OCDL). Figure 8A illustrates the means of detection using repair enzymes for a cluster containing a set bistranded base lesions as originally introduced by Sutherland, 2000. In one case, one of the lesions is a single strand break, SSB. With efficient repair and no cleavage of both strands at the site of the lesion, no detection of the cluster was seen. In scenario II, cleavage of both lesions by the enzyme induced a double strand break, DSB. The DSB provided detection of the cluster. Figure 8B displays detection of clusters using neutral agarose gel electrophoresis. DNA is subjected to agarose gel electrophoresis. With utilization of number average length analysis (NALA), the DSBs and OCDL were determined. A comparison is seen in the lanes with the enzyme and with the enzyme plus radiation. For lanes 1,2 (non-irradiated) low levels of endogenous OCDL are seen. For lanes 3,4 (irradiated) higher levels of OCDL are displayed. This is due to an increase in exogenous attacks from the radiation.

Comparison of lanes 3 and 1 provide the yield of DSBs. The same principle was utilized for the Lung Carcinoma and MCP-1 ko / B6 experiments to check for additional DSB formation upon treatment with the enzyme allowing us to quantify the clusters that are present.

Figure 9: Quantiscan Intensity Profile

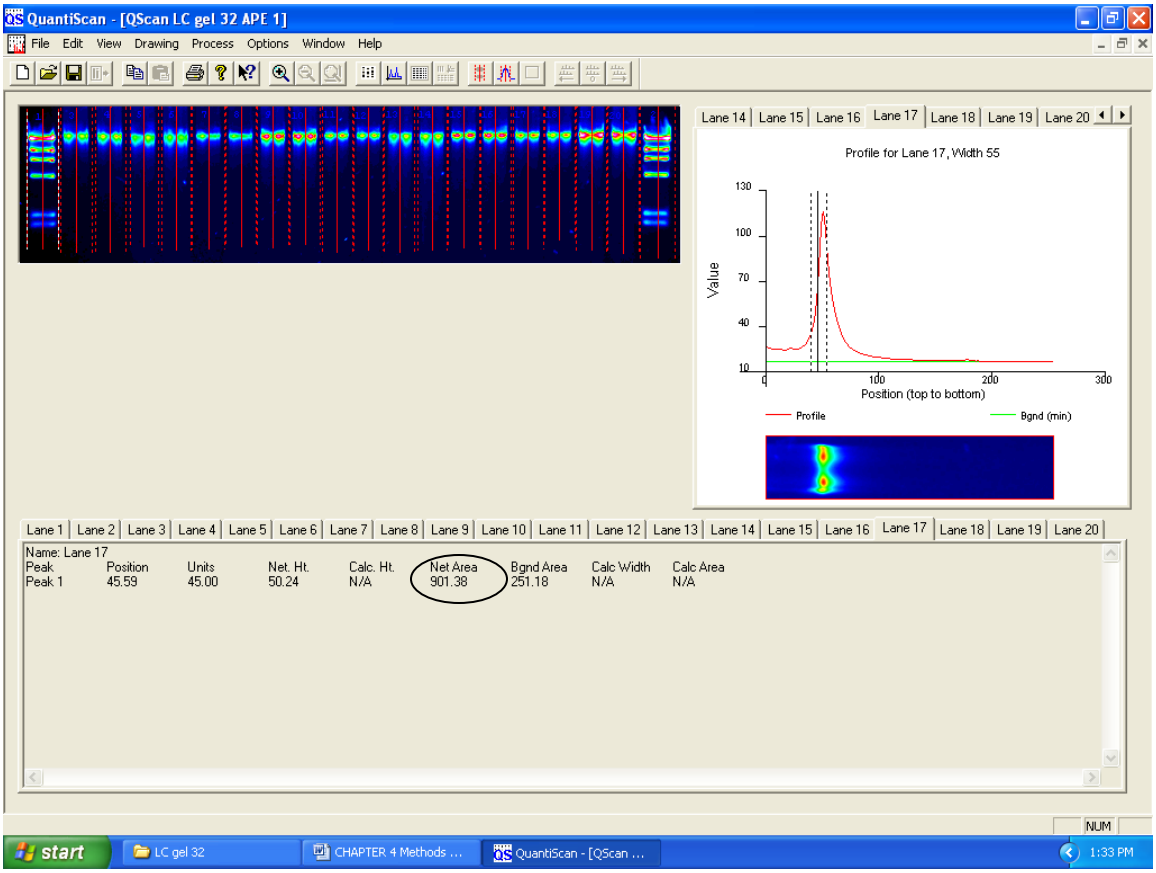

Figure 9: The figure displays a screen shot from Quantiscan. The intensity profile of a tumor bearing mouse sample with no enzyme treatment for the lung carcinoma experiment. The net area in circled. This corresponds to the intensity profile.

Figure 10: Origin Dispersion Curve

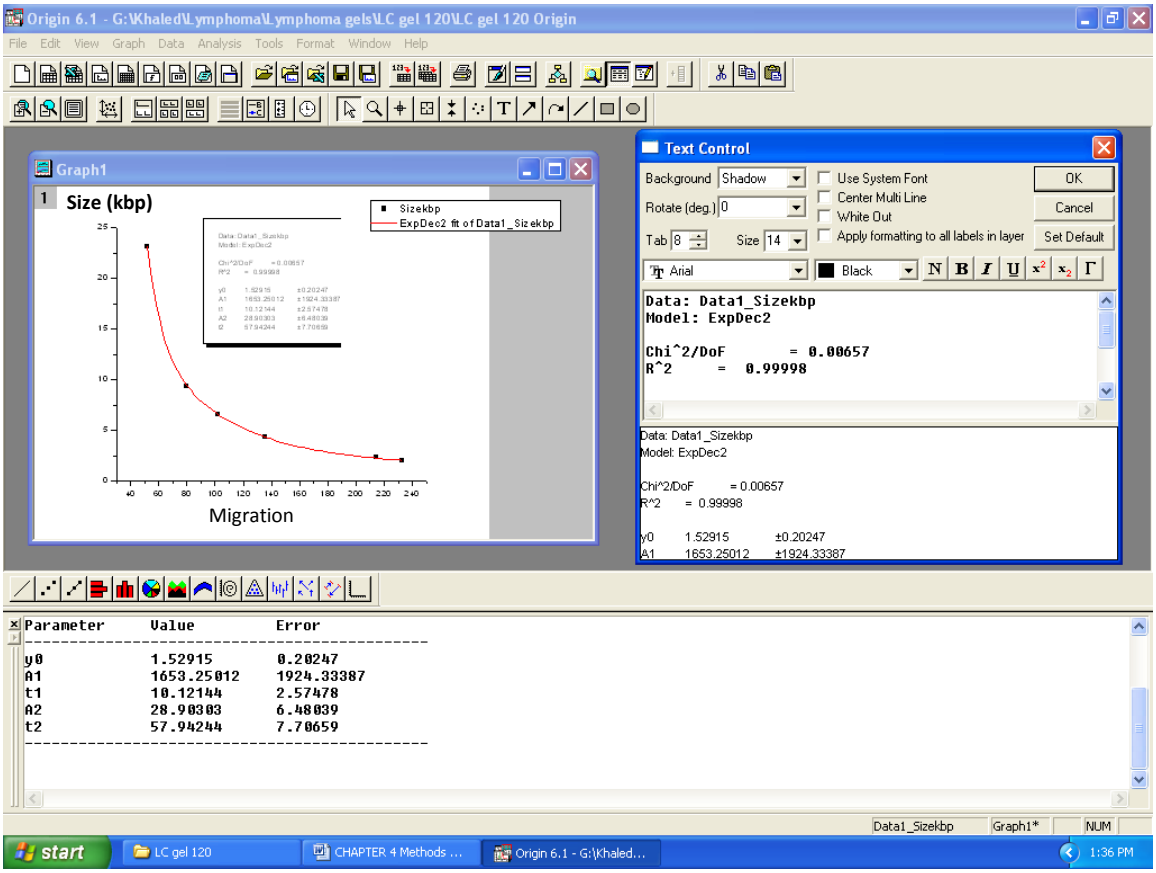

Figure 10: A corresponding size (kbp) vs Migration dispersion curve for the DNA marker, DNA λ–Hind III is illustrated above. Fragment size (kbp) corresponds to the *y* axis, and migration values correspond to the *x* axis. Plot was made using Origin Lab 6.0.

Figure 11: MS Excel Cluster Input

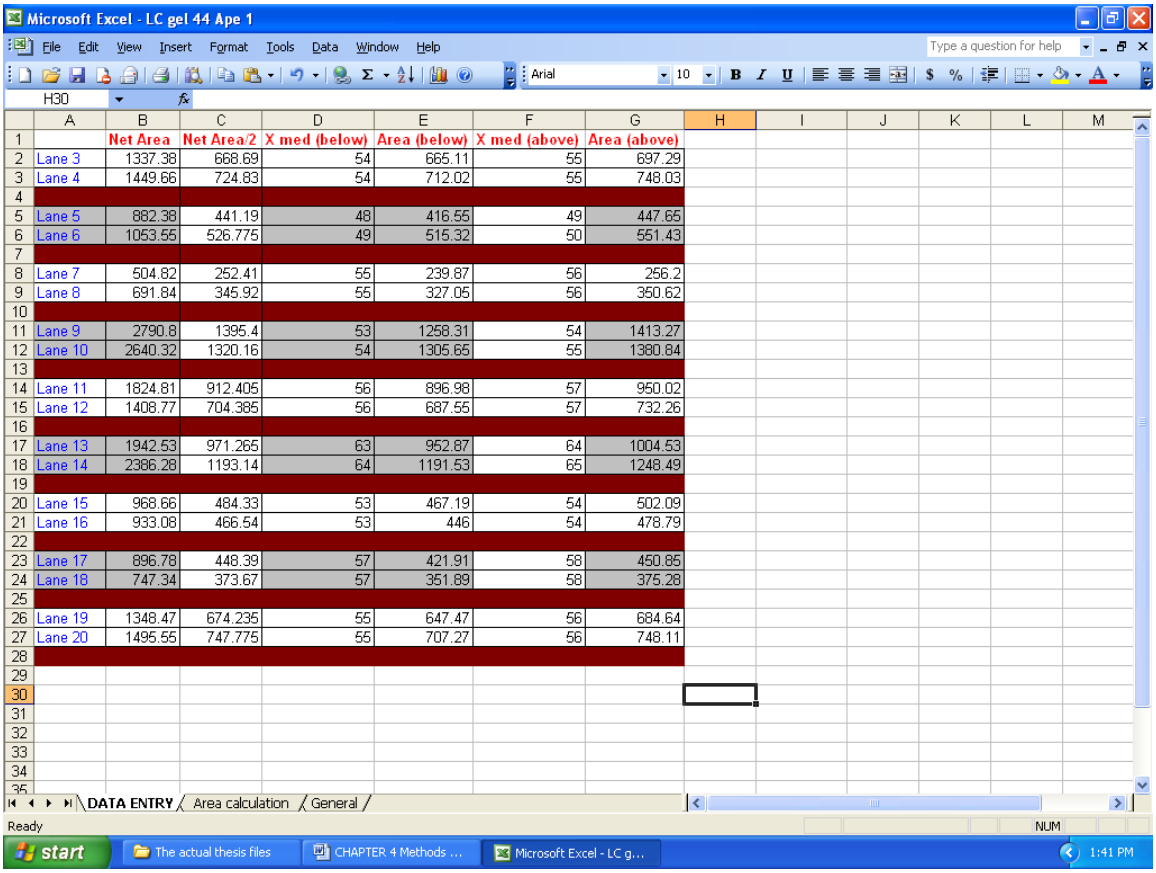

	A	B	C	D	E	F	G
1		Net Area	Net Area/2	X med (below)	Area (below)	X med (above)	Area (above)
2	Lane 3	1337.38	668.69	54	665.11	55	697.29
3	Lane 4	1449.66	724.83	54	712.02	55	748.03
4							
5	Lane 5	882.38	441.19	48	416.55	49	447.65
6	Lane 6	1053.55	526.775	49	515.32	50	551.43
7							
8	Lane 7	504.82	252.41	55	239.87	56	256.2
9	Lane 8	691.84	345.92	55	327.05	56	350.62
10							
11	Lane 9	2790.8	1395.4	53	1258.31	54	1413.27
12	Lane 10	2640.32	1320.16	54	1305.65	55	1380.84
13							
14	Lane 11	1824.81	912.405	56	896.98	57	950.02
15	Lane 12	1408.77	704.385	56	687.55	57	732.26
16							
17	Lane 13	1942.53	971.265	63	952.87	64	1004.53
18	Lane 14	2386.28	1193.14	64	1191.53	65	1248.49
19							
20	Lane 15	968.66	484.33	53	467.19	54	502.09
21	Lane 16	933.08	466.54	53	446	54	478.79
22							
23	Lane 17	896.78	448.39	57	421.91	58	450.85
24	Lane 18	747.34	373.67	57	351.89	58	375.28
25							
26	Lane 19	1348.47	674.235	55	647.47	56	684.64
27	Lane 20	1495.55	747.775	55	707.27	56	748.11
28							
29							
30							
31							
32							
33							
34							
35							

Figure 11: Upon determination of the net area, the value is entered in the data entry sheet. The area and migration coordinates that fall above and below the net area/2 are entered as well. The equation Ln=0.6 Lmed was utilized.

Figure 12: Ms Excel Area Calculation

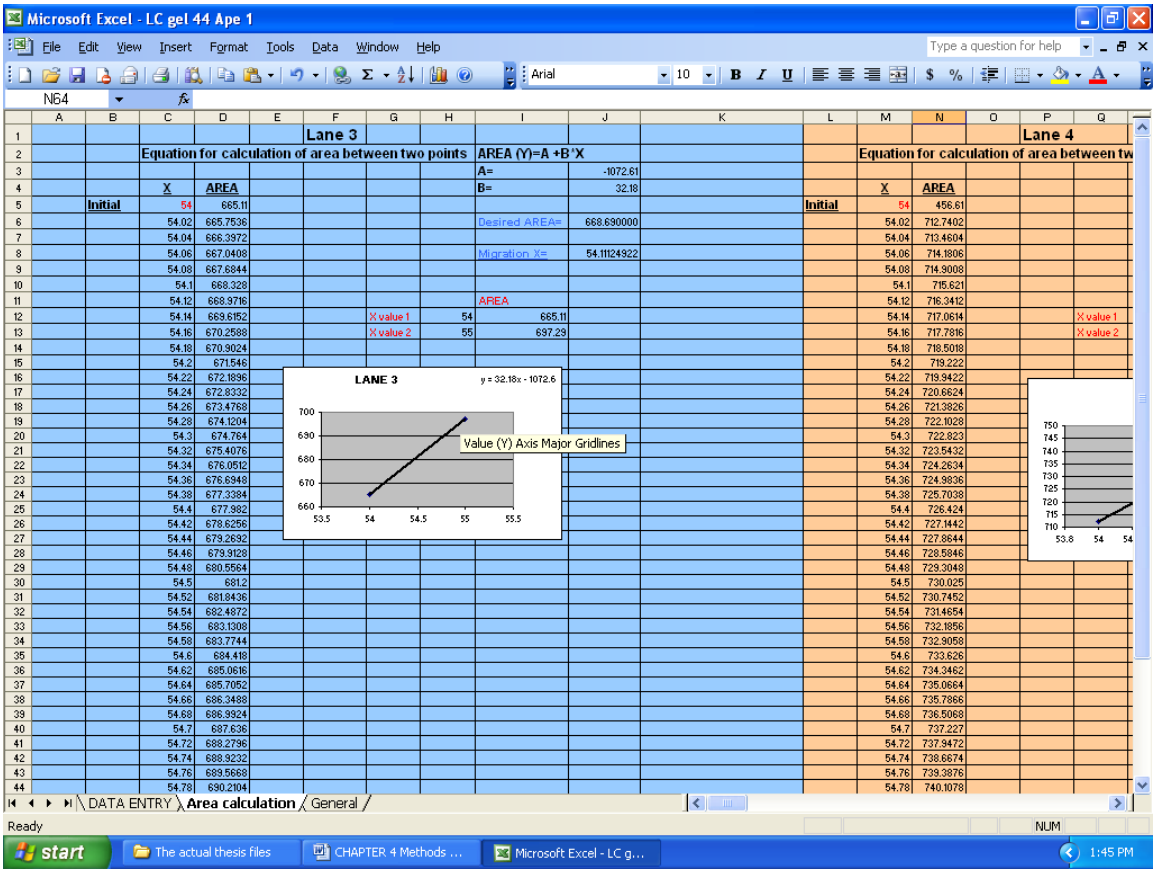

Figure 12: The precise x_{med} center from the intensity profile in quantiscan is calculated to 6 decimal places.

Figure 13: Ms Excel Cluster Calculation (Output)

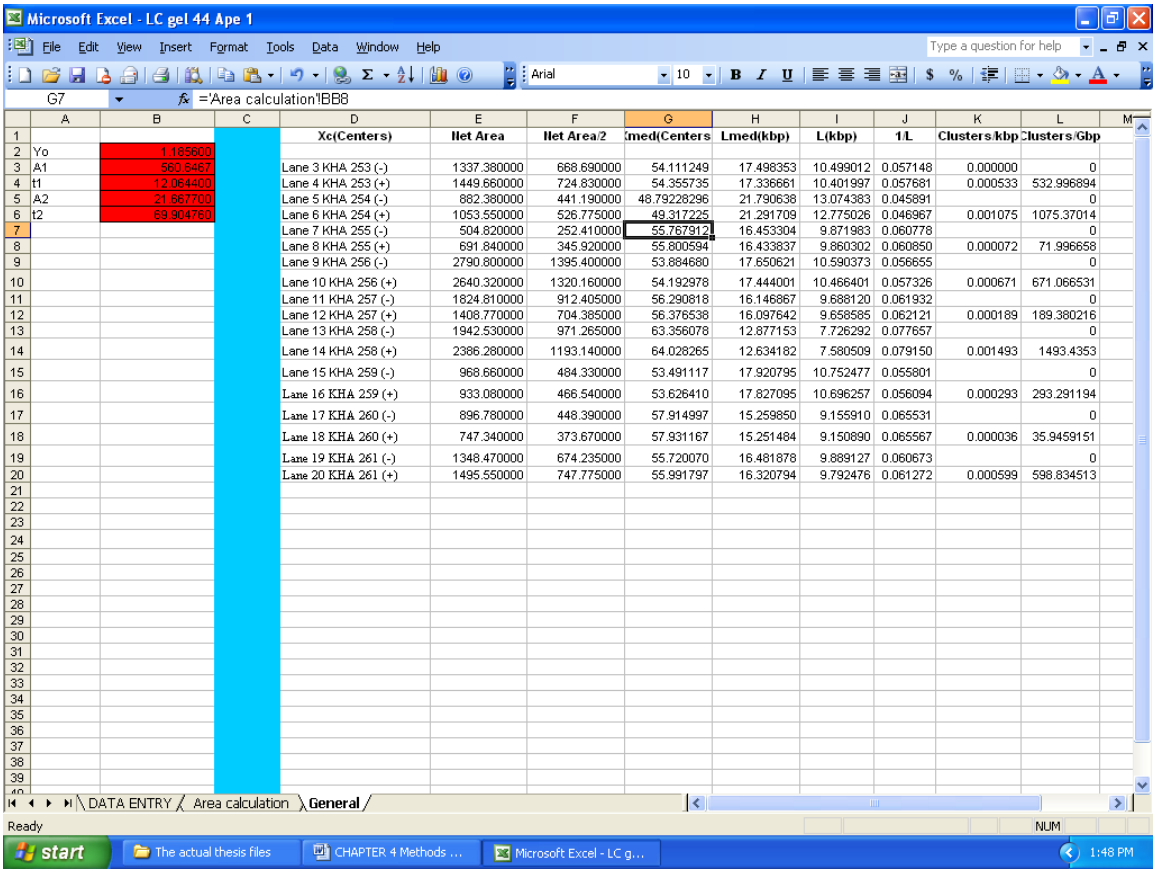

	A	B	C	D	E	F	G	H	I	J	K	L
1				Xc(Centers)	Net Area	Net Area/2	Lmed(Centers	Lmed(kbp)	L(kbp)	1/L	Clusters/kbp	Clusters/Gbp
2	Yo	1.185600										
3	A1	560.6467		Lane 3 KHA 253 (-)	1337.380000	668.690000	54.111249	17.498353	10.499012	0.057148	0.000000	0
4	t1	12.064400		Lane 4 KHA 253 (+)	1449.660000	724.830000	54.355735	17.336661	10.401997	0.057681	0.000533	532.996894
5	A2	21.667700		Lane 5 KHA 254 (-)	882.380000	441.190000	48.79228296	21.790638	13.074383	0.045891		0
6	t2	69.904760		Lane 6 KHA 254 (+)	1053.550000	526.775000	49.317225	21.291709	12.775026	0.046967	0.001075	1075.37014
7				Lane 7 KHA 255 (-)	504.820000	252.410000	55.767912	16.453304	9.871983	0.060778		0
8				Lane 8 KHA 255 (+)	691.840000	345.920000	55.800594	16.433837	9.860302	0.060850	0.000072	71.996658
9				Lane 9 KHA 256 (-)	2790.800000	1395.400000	53.884680	17.650621	10.590373	0.056655		0
10				Lane 10 KHA 256 (+)	2640.320000	1320.160000	54.192978	17.444001	10.466401	0.057326	0.000671	671.066531
11				Lane 11 KHA 257 (-)	1824.810000	912.405000	56.290818	16.146867	9.688120	0.061932		0
12				Lane 12 KHA 257 (+)	1408.770000	704.385000	56.376538	16.097642	9.658585	0.062121	0.000189	189.380216
13				Lane 13 KHA 258 (-)	1942.530000	971.265000	63.356078	12.877153	7.726292	0.077657		0
14				Lane 14 KHA 258 (+)	2386.280000	1193.140000	64.028265	12.634182	7.580509	0.079150	0.001493	1493.4353
15				Lane 15 KHA 259 (-)	968.660000	484.330000	53.491117	17.920795	10.752477	0.055801		0
16				Lane 16 KHA 259 (+)	933.080000	466.540000	53.626410	17.827095	10.696257	0.056094	0.000293	293.291194
17				Lane 17 KHA 260 (-)	896.780000	448.390000	57.914997	15.259850	9.155910	0.065531		0
18				Lane 18 KHA 260 (+)	747.340000	373.670000	57.931167	15.251484	9.150890	0.065567	0.000036	35.9459151
19				Lane 19 KHA 261 (-)	1348.470000	674.235000	55.720070	16.481878	9.889127	0.060673		0
20				Lane 20 KHA 261 (+)	1495.550000	747.775000	55.991797	16.320794	9.792476	0.061272	0.000599	598.834513

Figure 13: Equation {4} from Sutherland *et al*, yields the number of clusters (Column L : Row 4). The parameters obtained using Origin 6.0 are entered in the cells labeled in red. Cluster values are provided in Gbp. Determine number of clusters (Φ) using the equation: $\Phi=1/L_T-1/L_{U;}$ Example (Lane 4 – Lane 5).

CHAPTER 5: RESULTS

The data that was obtained from the lung carcinoma experiment are shown in figures 13-23. Figures 24-26 exhibit a cumulative analysis per enzyme treatment of the tissues that were utilized for the lung carcinoma experiment. To determine the existence of significant differences between different cohorts and groups of mice, A t test was executed at a significance level of $p<0.05$. The different comparisons were as follows: nude mice with lung carcinoma (TST) vs. inflammation control; nude mice TST vs. nude mice TST + Tempol; nude mice TST vs. B6 TST mice. The OCDL experiments were carried out a minimum of three repetitions per enzyme per sample. In general, a trend is seen with an increase in cluster accumulation for the mice bearing lung carcinoma compared to the inflammation control and the PBS control. This increase of clusters is also seen to significantly decrease with the presence of the antioxidant Tempol. Proximity to the tumor shows no significant difference in cluster formation. This implies that the bystander effect is indeed being carried out. The damage detected in B6 mice bearing lung carcinoma vs. nude mice with lung carcinoma varied. This implies that a fully functioning immune system will not completely eradicate the damage associated from endogenous sources.

The data obtained from the MCP-1 ko and B6 experiments are shown in figures 27-30. Figures 31-33 exhibit a cumulative analysis per enzyme treatment of the tissues that were utilized for the MCP-1 ko and B6 experiment. Four statistical t-tests were performed at significance level of $p<0.05$ to examine the differences between the different cohorts and samples. They are as follows: MCP-1 ko inflammation control vs. MCP-1 ko TST (Melanoma); MCP-1 ko inflammation control vs. MCP-1 ko TST (Sarcoma); MCP-1 ko TST (Melanoma) vs. B6 TST (Melanoma); and MCP-1 ko TST (Sarcoma) vs. B6 TST (Sarcoma). The OCDL experiment was carried out a minimum of three repetitions per enzyme per sample. In general it

was seen that when MCP-1 was knocked out, there is a decrease in cluster damage. This implements the role of MCP-1 as a key component to cluster damage which corresponds to the findings performed by Redon *et al* (Redon *et al*, 2010). When compared to B6 mice bearing the different tumors, MCP-1 ko tumor bearing mice exhibit a general decrease in damage.

Figure 14: Cluster Analysis in Ovary Tissues - Lung Carcinoma Experiment

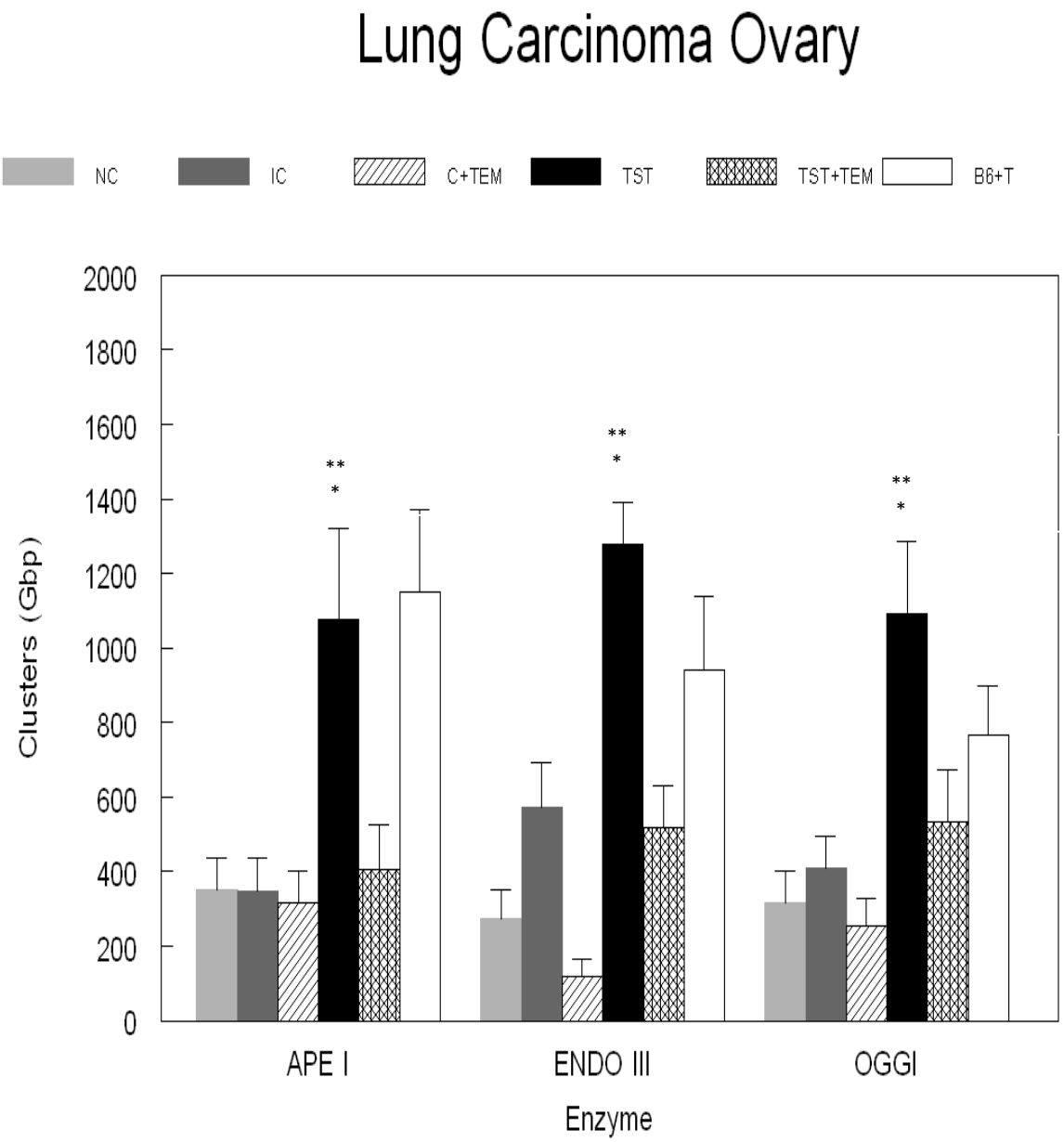

Figure 14: Cluster damage detected in ovary tissue samples from lung carcinoma experiment for the three different enzymes that were utilized. The Y axis corresponds to the number of clusters (Gbp) and the X axis corresponds to the three different enzymes. Significant cluster accumulation between nude mice TST and inflammation control mice at $p<0.05$ is denoted by *. Significant difference between nude mice TST and nude mice TST + Tempol is denoted by **. Significant difference between nude mice TST and B6 TST mice is denoted by ***.

Figure 15: Cluster Analysis in Lung Tissues - Lung Carcinoma Experiment

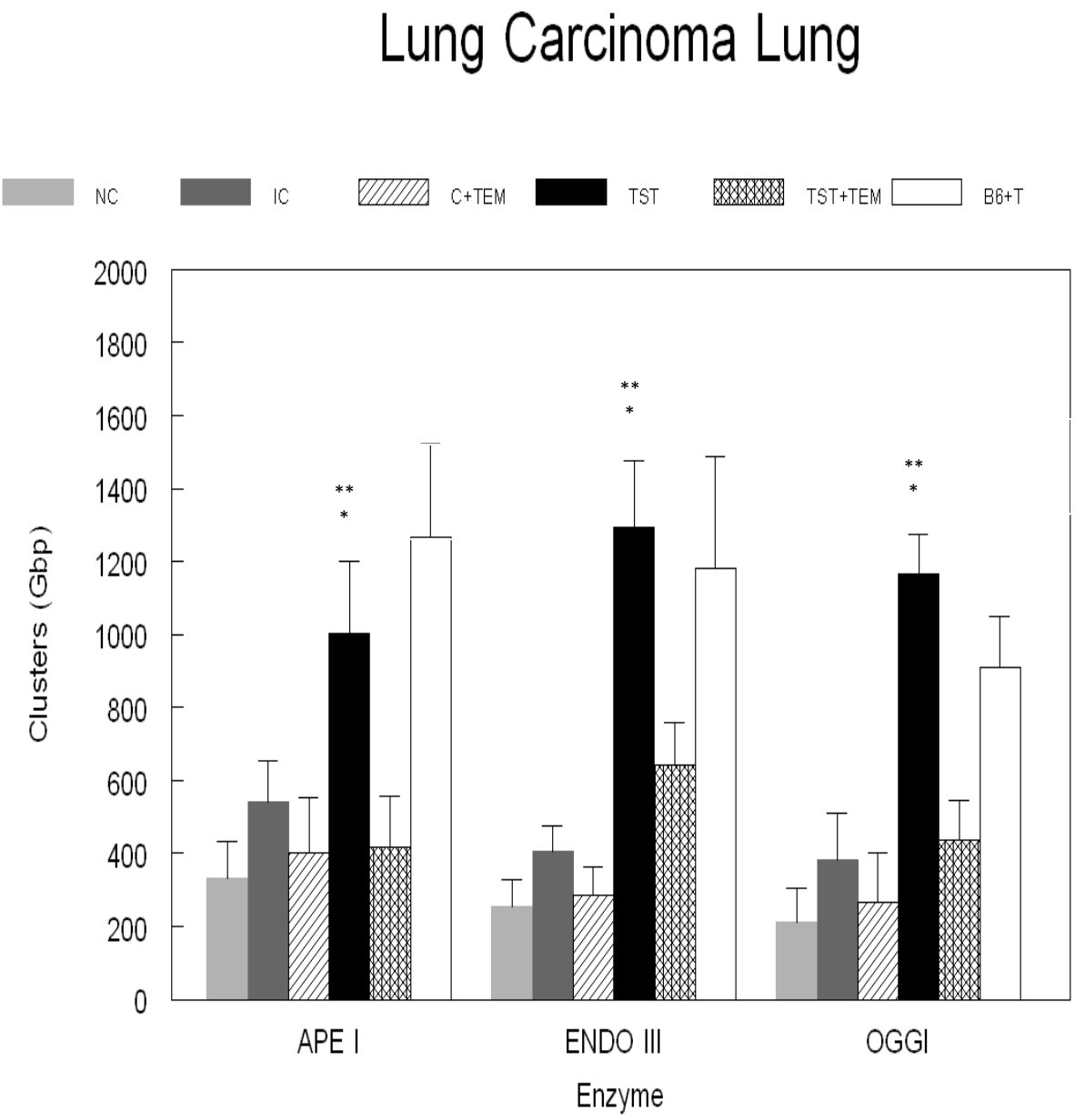

Figure 15: Cluster damage detected in lung tissue samples from Lung Carcinoma experiment for the three different enzymes that were utilized. The Y axis corresponds to the number of clusters (Gbp) and the X axis corresponds to the three different enzymes. Significant cluster accumulation between nude mice TST and inflammation control mice at $p<0.05$ is denoted by *. Significant difference between nude mice TST and nude mice TST + Tempol is denoted by **. Significant difference between nude mice TST and B6 TST mice is denoted by ***.

Figure 16: Cluster Analysis in Spleen Tissues - Lung Carcinoma Experiment

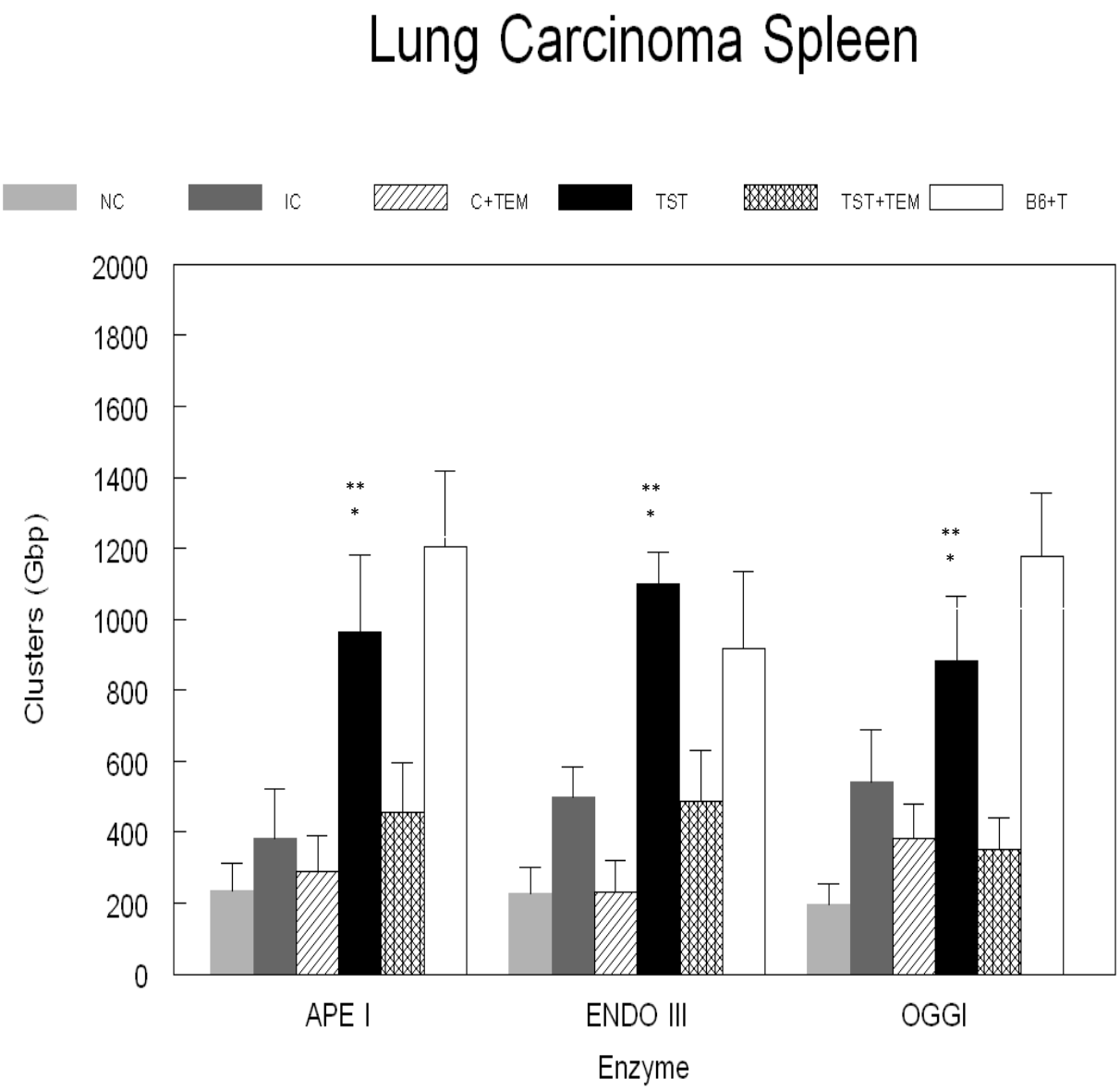

Figure 16: Cluster damage detected in spleen tissue samples from Lung Carcinoma experiment for the three different enzymes that were utilized. The Y axis corresponds to the number of clusters (Gbp) and the X axis corresponds to the three different enzymes. Significant cluster accumulation between nude mice TST and inflammation control mice at $p<0.05$ is denoted by *. Significant difference between nude mice TST and nude mice TST + Tempol is denoted by **. Significant difference between nude mice TST and B6 TST mice is denoted by ***.

Figure 17: Cluster Analysis in Duodenum Tissues - Lung Carcinoma Experiment

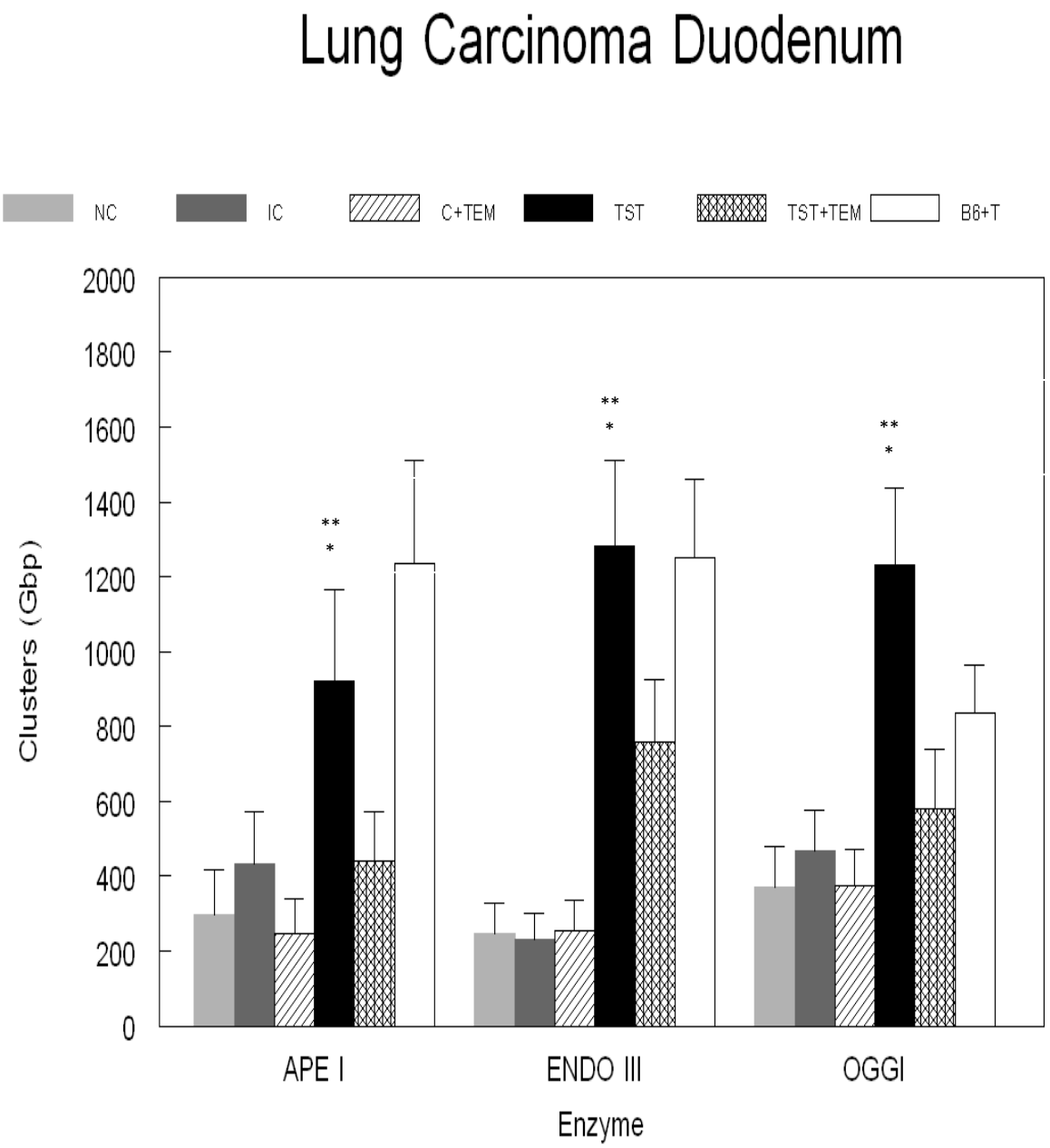

Figure 17: Cluster damage detected in duodenum tissue samples from Lung Carcinoma experiment for the three different enzymes that were utilized. The Y axis corresponds to the number of clusters (Gbp) and the X axis corresponds to the three different enzymes. Significant cluster accumulation between nude mice TST and inflammation control mice at $p<0.05$ is denoted by *. Significant difference between nude mice TST and nude mice TST + Tempol is denoted by **. Significant difference between nude mice TST and B6 TST mice is denoted by ***.

Figure 18: Cluster Analysis in Stomach Tissues - Lung Carcinoma Experiment

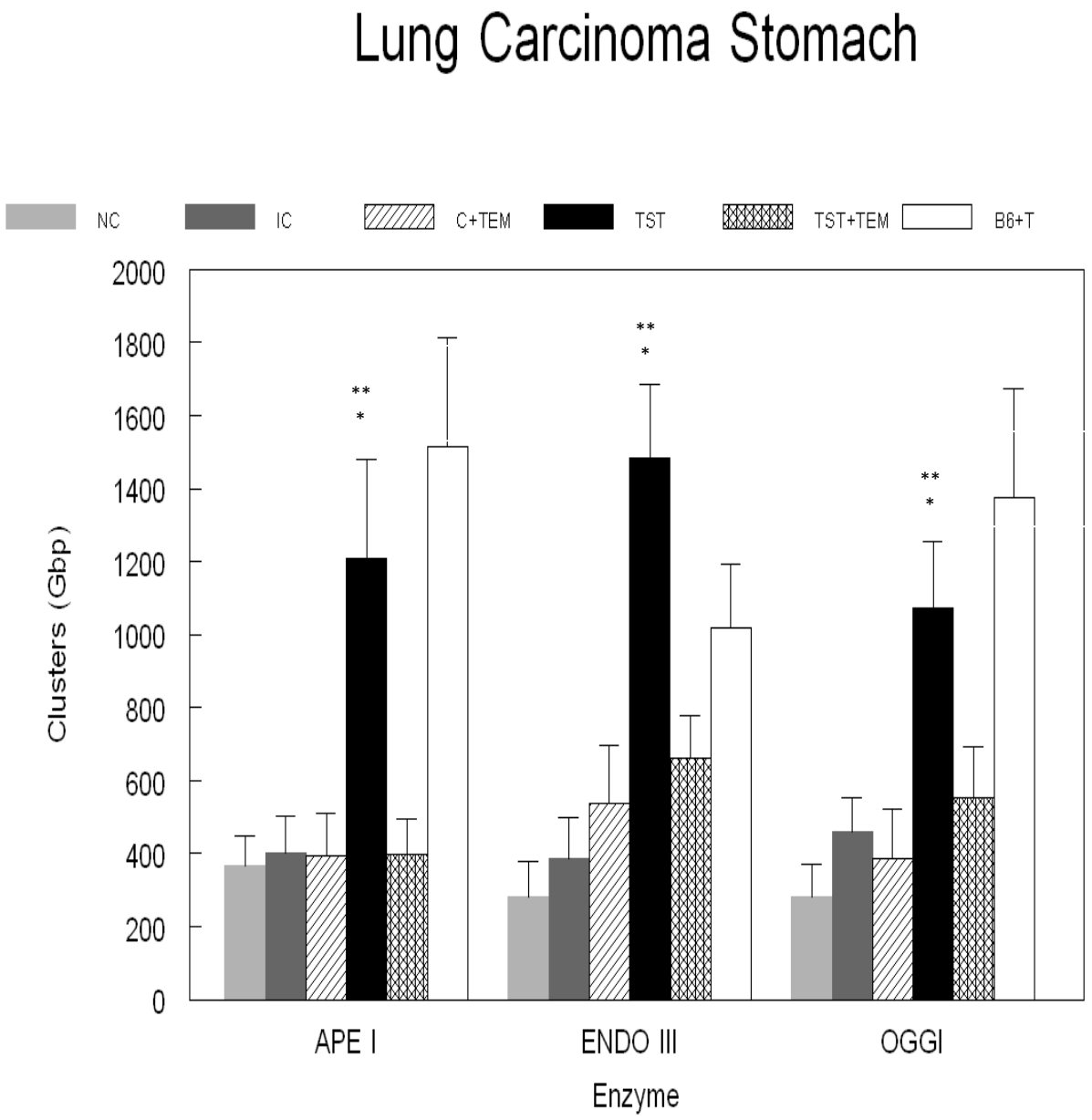

Figure 18: Cluster damage detected in stomach tissue samples from Lung Carcinoma experiment for the three different enzymes that were utilized. The Y axis corresponds to the number of clusters (Gbp) and the X axis corresponds to the three different enzymes. Significant cluster accumulation between nude mice TST and inflammation control mice at $p<0.05$ is denoted by *. Significant difference between nude mice TST and nude mice TST + Tempol is denoted by **. Significant difference between nude mice TST and B6 TST mice is denoted by ***.

Figure 19: Cluster Analysis in Colon Tissues - Lung Carcinoma Experiment

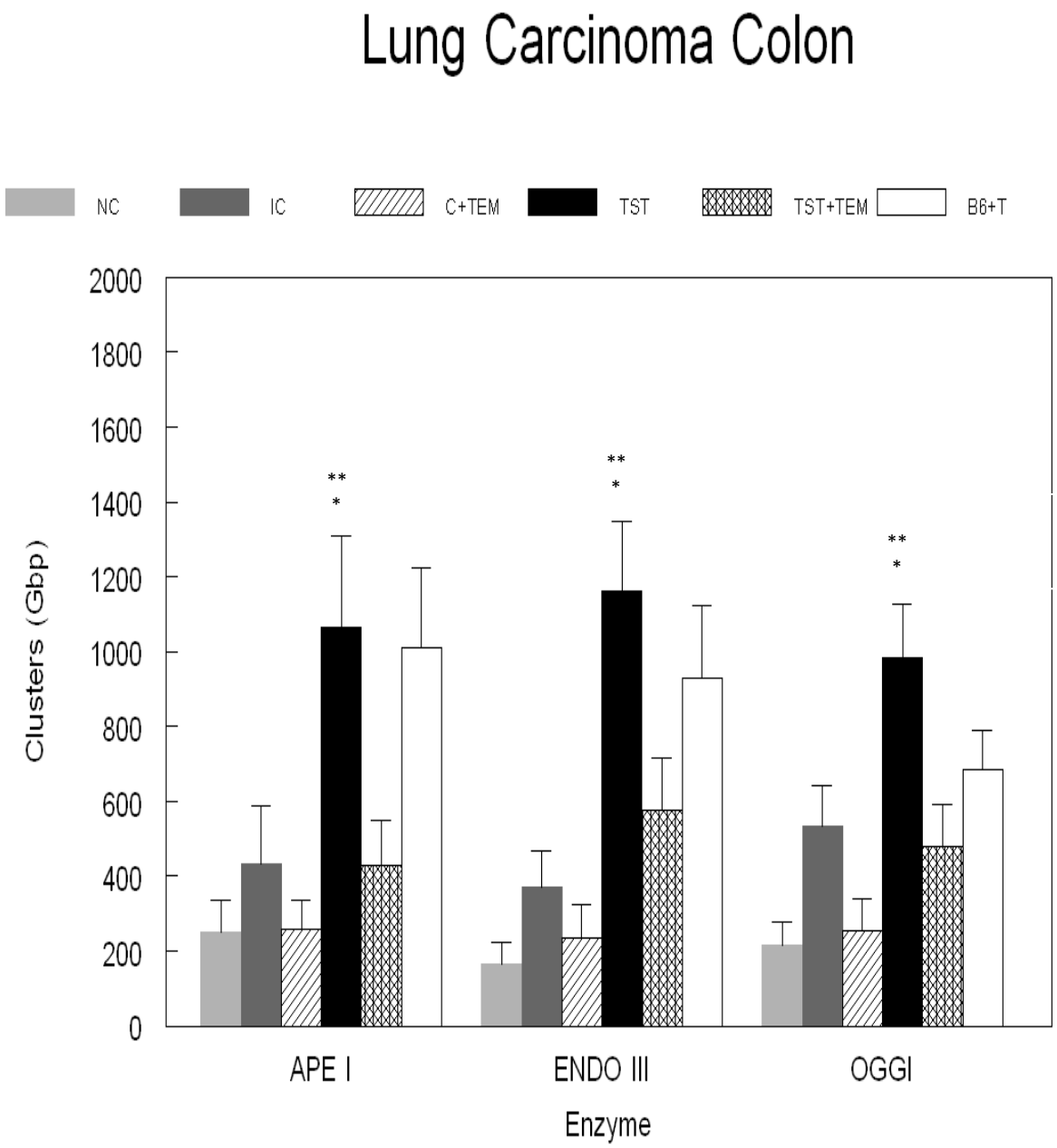

Figure 19: Cluster damage detected in colon tissue samples from Lung Carcinoma experiment for the three different enzymes that were utilized. The Y axis corresponds to the number of clusters (Gbp) and the X axis corresponds to the three different enzymes. Significant cluster accumulation between nude mice TST and inflammation control mice at $p<0.05$ is denoted by *. Significant difference between nude mice TST and nude mice TST + Tempol is denoted by **. Significant difference between nude mice TST and B6 TST mice is denoted by ***.

Figure 20: Cluster Analysis in Rectum Tissues - Lung Carcinoma Experiment

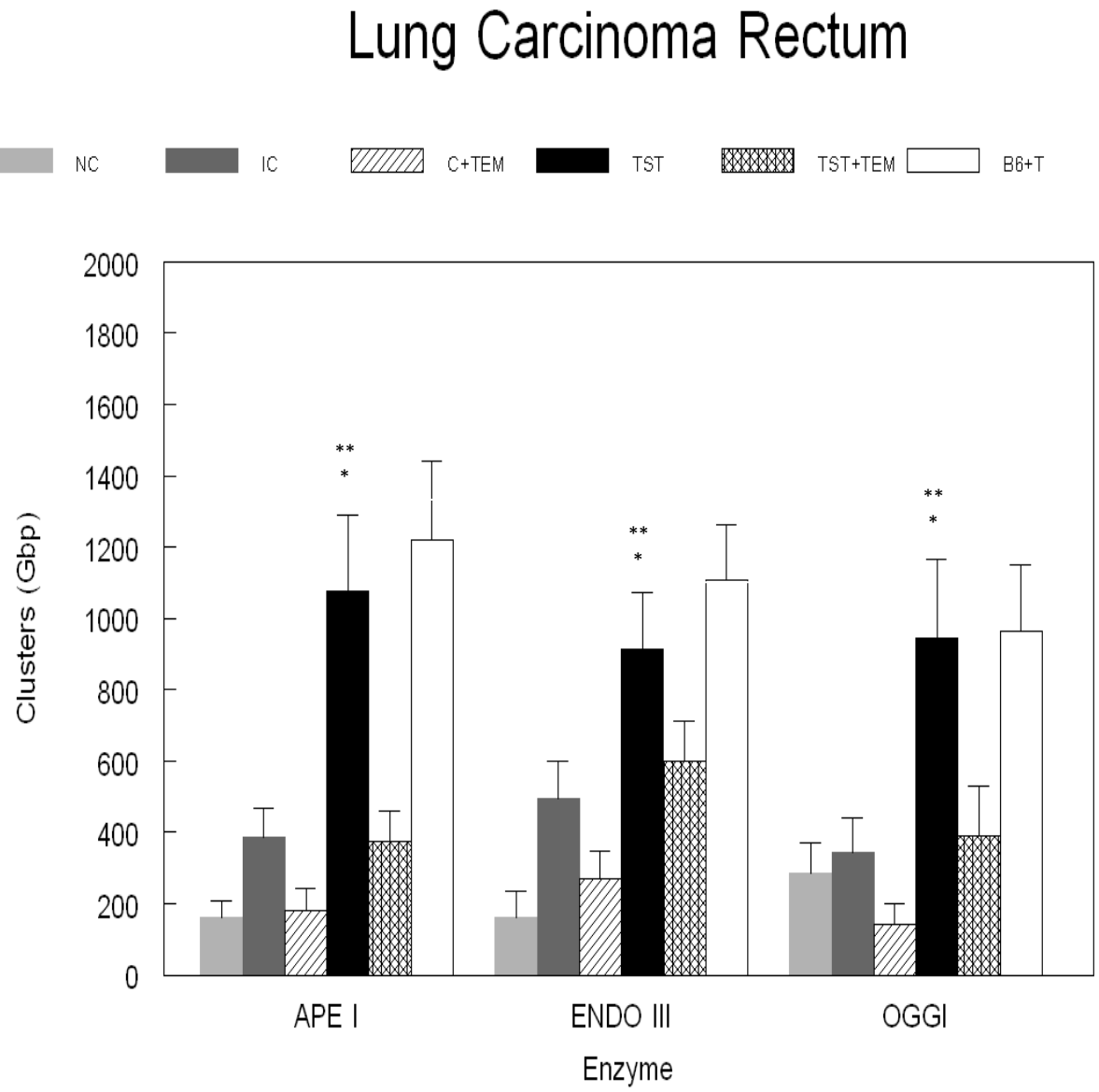

Figure 20: Cluster damage detected in rectum tissue samples from Lung Carcinoma experiment for the three different enzymes that were utilized. The Y axis corresponds to the number of clusters (Gbp) and the X axis corresponds to the three different enzymes. Significant cluster accumulation between nude mice TST and inflammation control mice at $p<0.05$ is denoted by *. Significant difference between nude mice TST and nude mice TST + Tempol is denoted by **. Significant difference between nude mice TST and B6 TST mice is denoted by ***.

Figure 21: Cluster Analysis in Skin (Lateral) Tissues - Lung Carcinoma Experiment

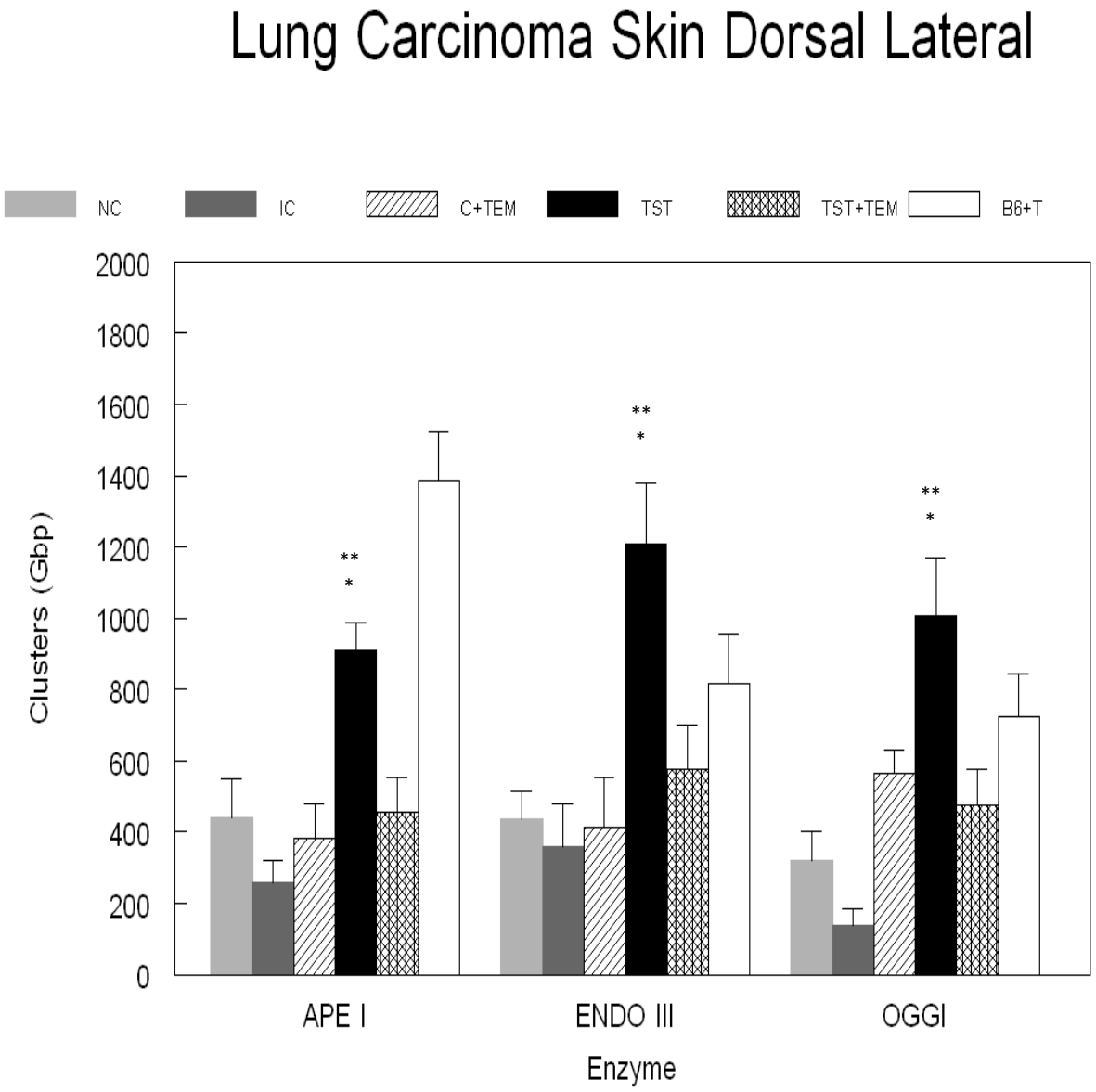

Figure 21: Cluster damage detected in skin (lateral) tissue samples from Lung Carcinoma experiment for the three different enzymes that were utilized. The Y axis corresponds to the number of clusters (Gbp) and the X axis corresponds to the three different enzymes. Significant cluster accumulation between nude mice TST and inflammation control mice at $p<0.05$ is denoted by *. Significant difference between nude mice TST and nude mice TST + Tempol is denoted by **. Significant difference between nude mice TST and B6 TST mice is denoted by ***.

Figure 22: Cluster Analysis in Skin (Cervical) Tissues - Lung Carcinoma Experiment

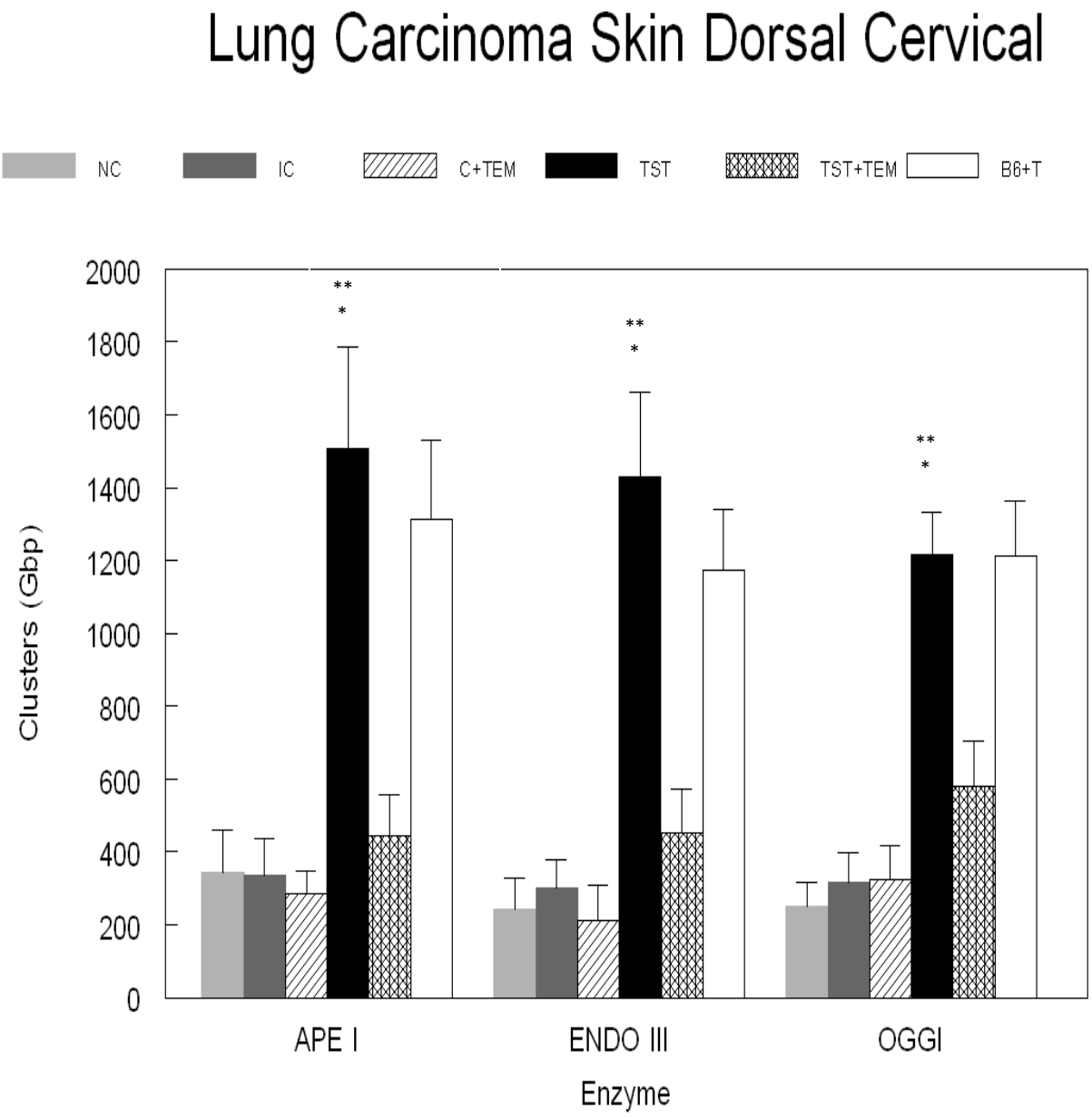

Figure 22: Cluster damage detected in skin (cervical) tissue samples from Lung Carcinoma experiment for the three different enzymes that were utilized. The Y axis corresponds to the number of clusters (Gbp) and the X axis corresponds to the three different enzymes. Significant cluster accumulation between nude mice TST and inflammation control mice at $p<0.05$ is denoted by *. Significant difference between nude mice TST and nude mice TST + Tempol is denoted by **. Significant difference between nude mice TST and B6 TST mice is denoted by ***.

Figure 23: Cluster Analysis in Skin (Tumor mass) Tissues - Lung Carcinoma Experiment

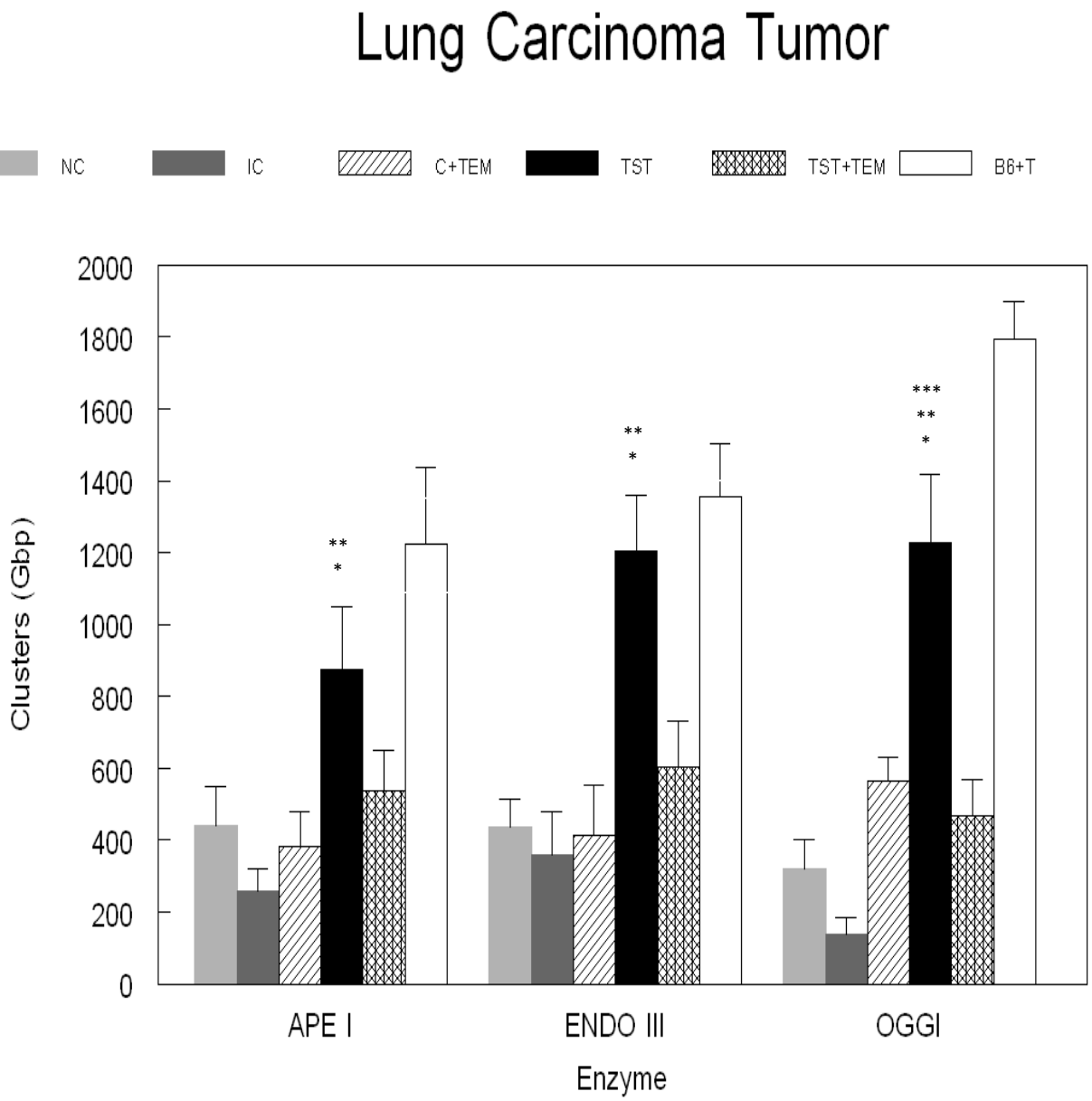

Figure 23: Cluster damage detected in skin (tumor mass) tissue samples from Lung Carcinoma experiment for the three different enzymes that were utilized. The Y axis corresponds to the number of clusters (Gbp) and the X axis corresponds to the three different enzymes. Significant cluster accumulation between nude mice TST and inflammation control mice at $p<0.05$ is denoted by *. Significant difference between nude mice TST and nude mice TST + Tempol is denoted by **. Significant difference between nude mice TST and B6 TST mice is denoted by ***.

Figure 24: Abasic Cluster Analysis - Lung Carcinoma Experiment

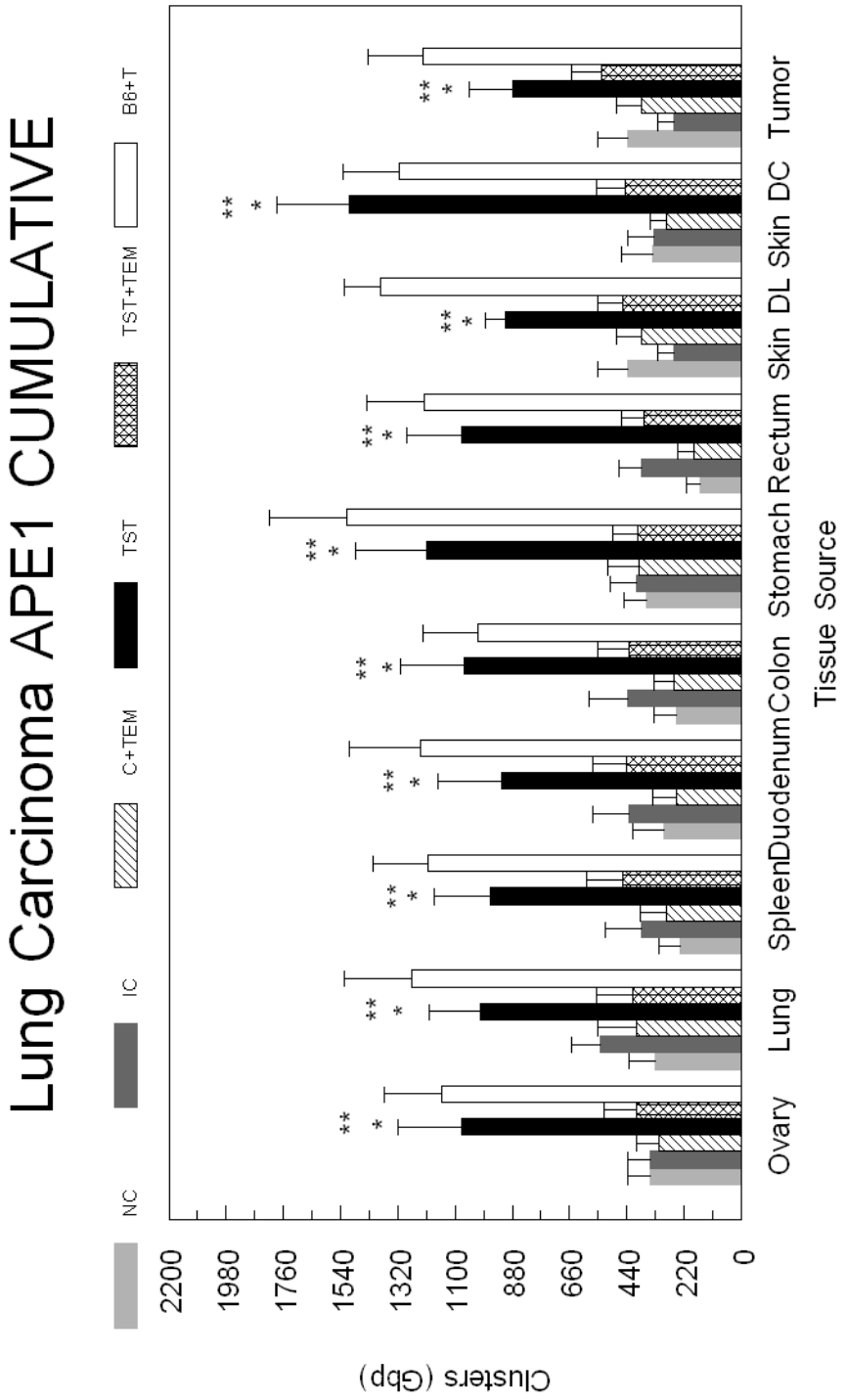

Figure 24: Abasic clusters that were detected from the Lung Carcinoma Experiment. Significant cluster accumulation between nude mice TST and inflammation control mice at $p<0.05$ is denoted by *. Significant difference between nude mice TST and nude mice TST + Tempol is denoted by **. Significant difference between nude mice TST and B6 TST mice is denoted by ***.

Figure 25: Oxypyrimidinic Cluster Analysis - Lung Carcinoma Experiment

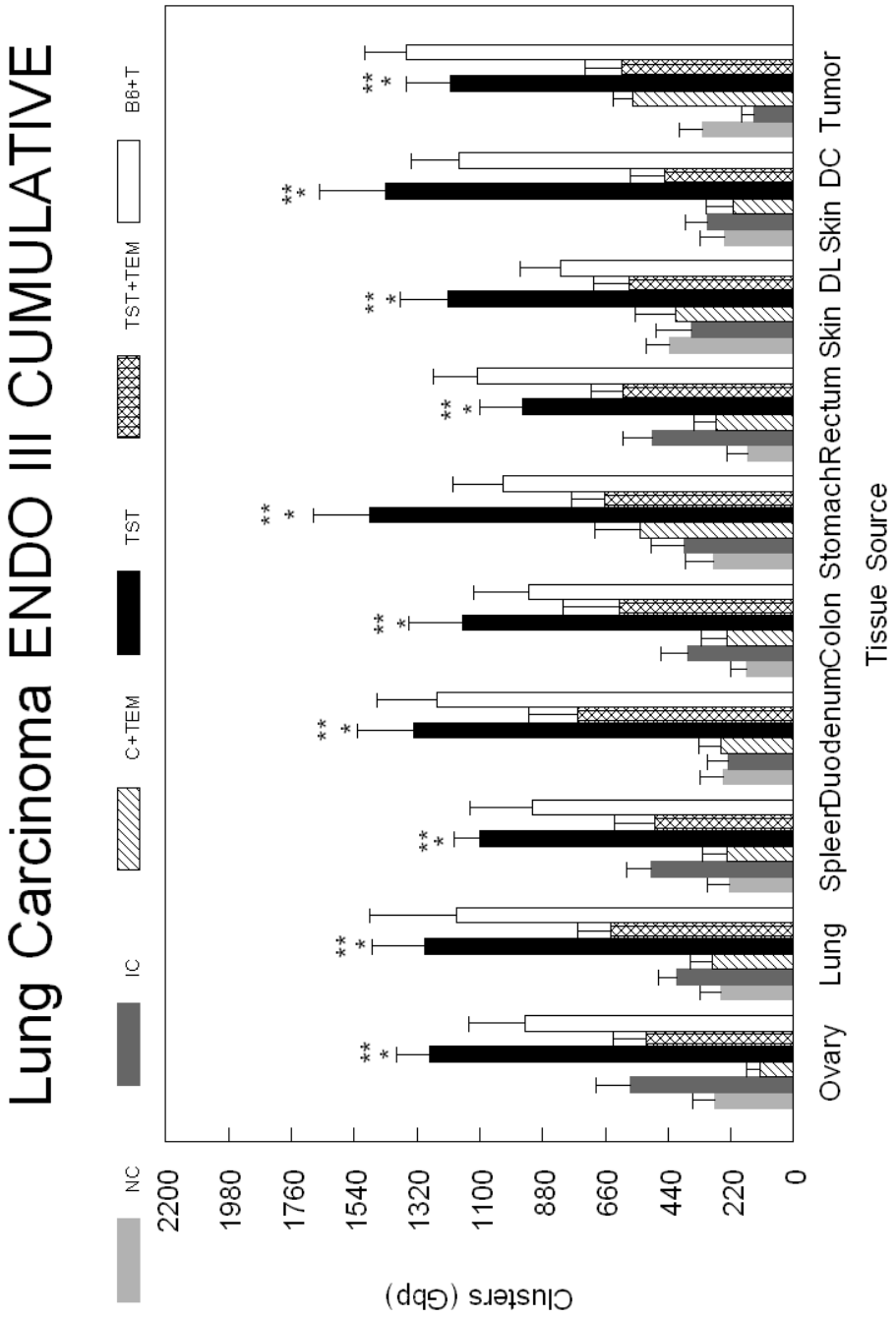

Figure 25: Oxypyrimidinic clusters that were detected from the Lung Carcinoma Experiment. Significant cluster accumulation between nude mice TST and inflammation control mice at $p<0.05$ is denoted by *. Significant difference between nude mice TST and nude mice TST + Tempol is denoted by **. Significant difference between nude mice TST and B6 TST mice is denoted by ***.

Figure 26: Oxypurinic Cluster Analysis - Lung Carcinoma Experiment

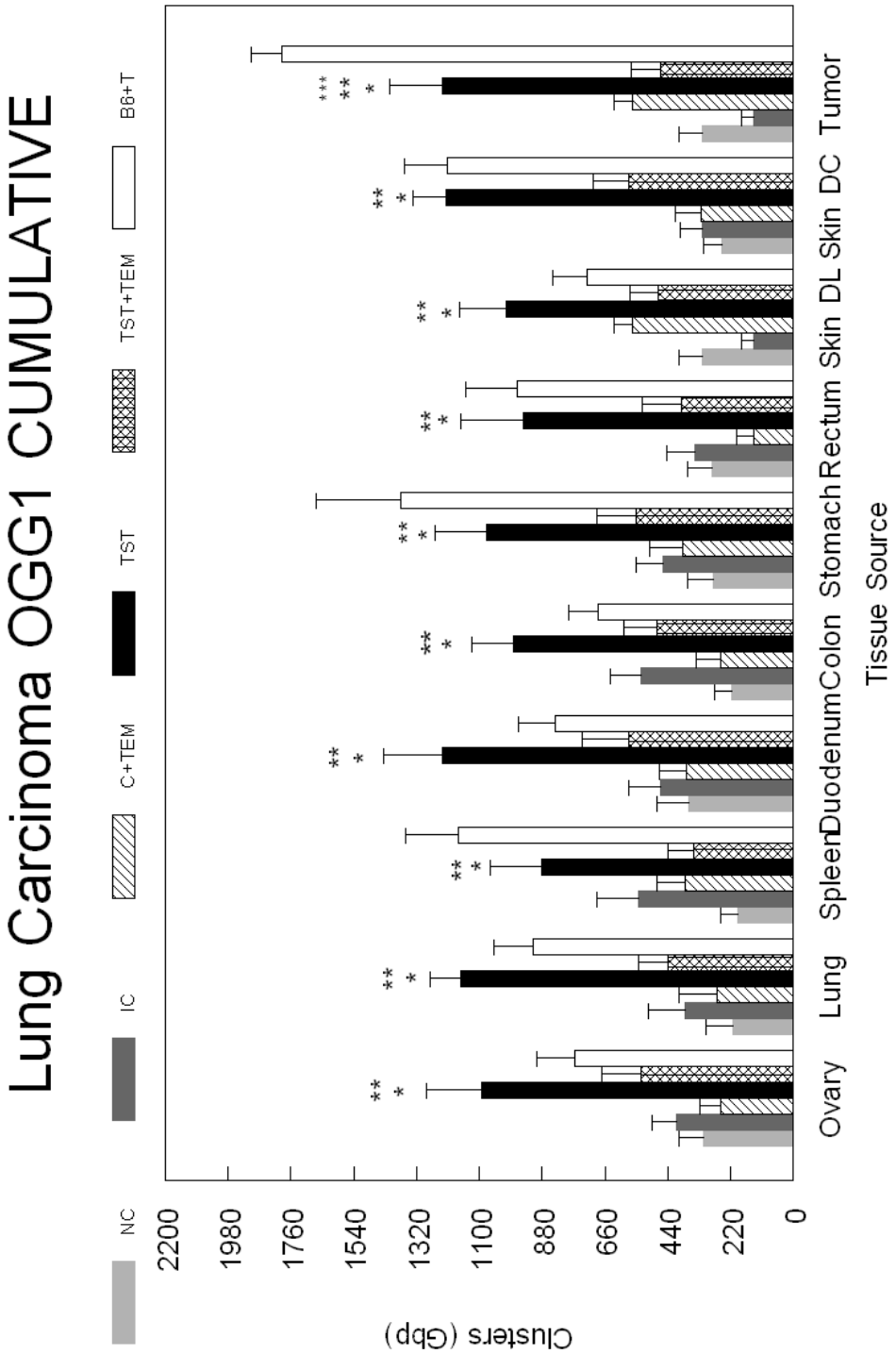

Figure 26: Oxypurinic clusters that were detected from the Lung Carcinoma Experiment. Significant cluster accumulation between nude mice TST and inflammation control mice at $p<0.05$ is denoted by *. Significant difference between nude mice TST and nude mice TST + Tempol is denoted by **. Significant difference between nude mice TST and B6 TST mice is denoted by ***.

Figure 27: Cluster Analysis in Colon – MCP-1 KO

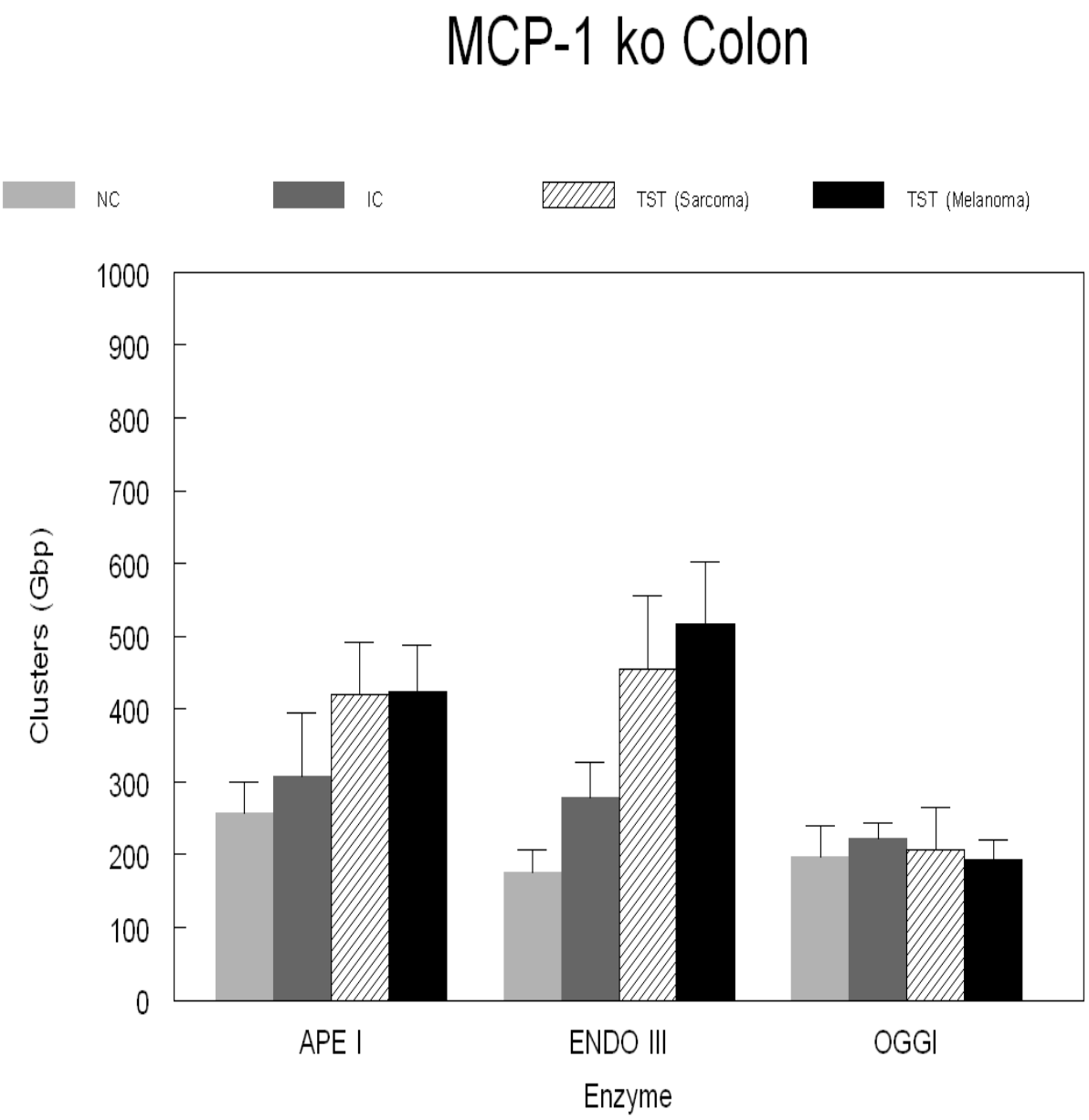

Figure 27: Cluster damage detected in colon tissue samples from the MCP-1 ko experiment for the three different enzymes that were utilized. The Y axis corresponds to the number of clusters (Gbp) and the X axis corresponds to the three different enzymes.

Figure 28: Cluster Analysis in Duodenum – MCP-1 KO

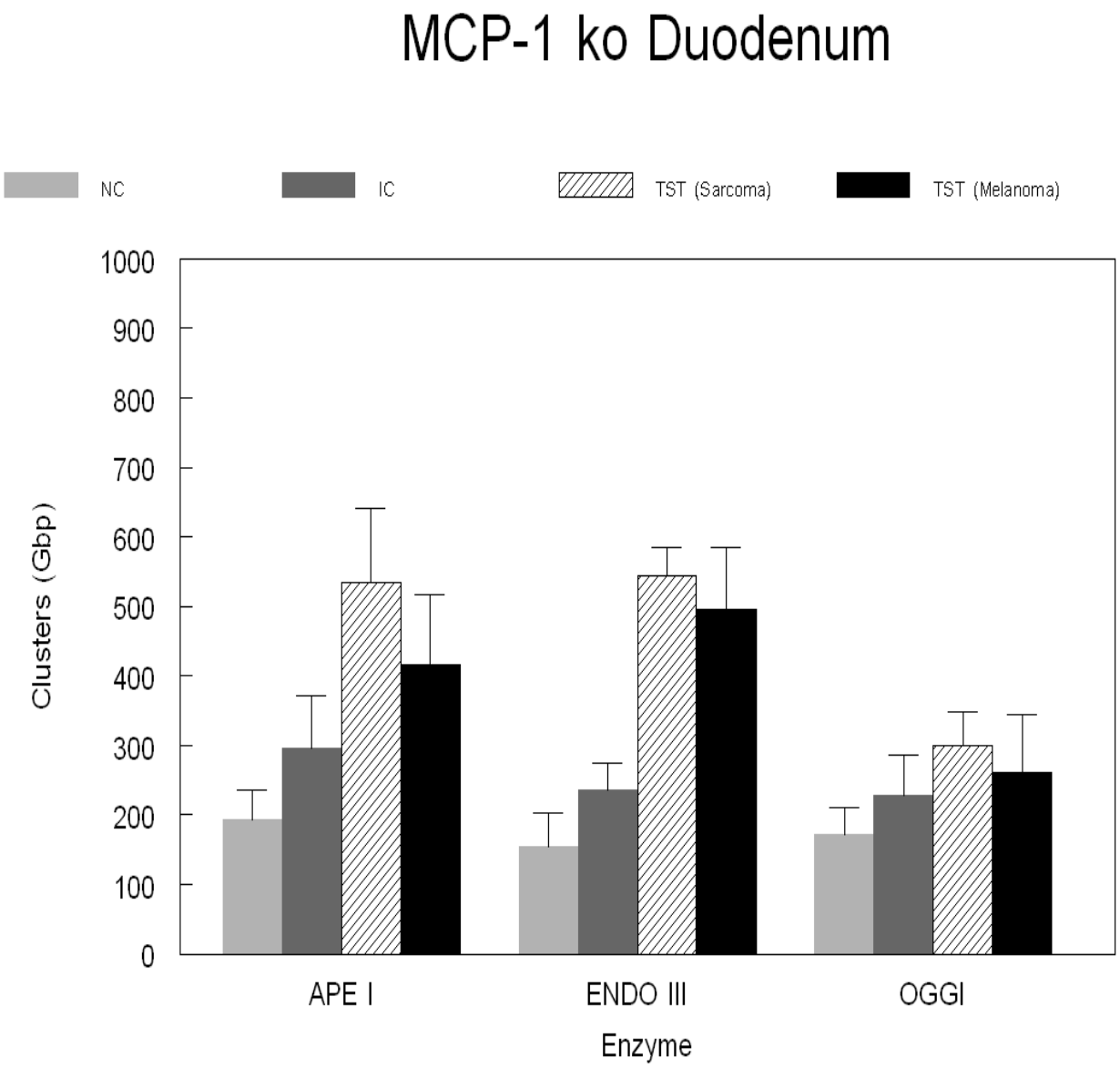

Figure 28: Cluster damage detected in duodenum tissue samples from the MCP-1 ko experiment for the three different enzymes that were utilized. The Y axis corresponds to the number of clusters (Gbp) and the X axis corresponds to the three different enzymes.

Figure 29: Cluster Analysis in Colon – B6

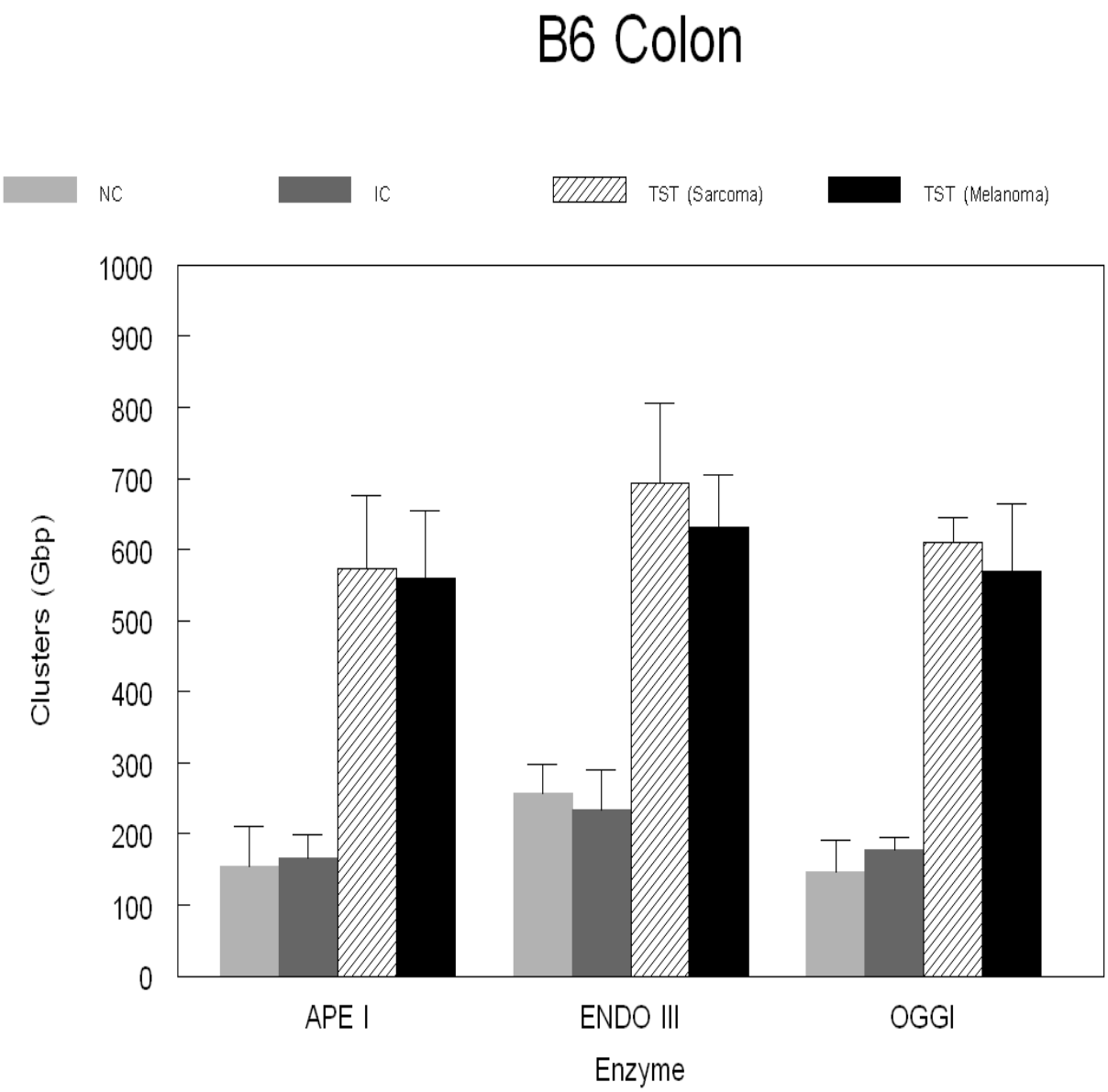

Figure 29: Cluster damage detected in colon tissue samples from the B6 experiment for the three different enzymes that were utilized. The Y axis corresponds to the number of clusters (Gbp) and the X axis corresponds to the three different enzymes.

Figure 30: Cluster Analysis in Duodenum – B6

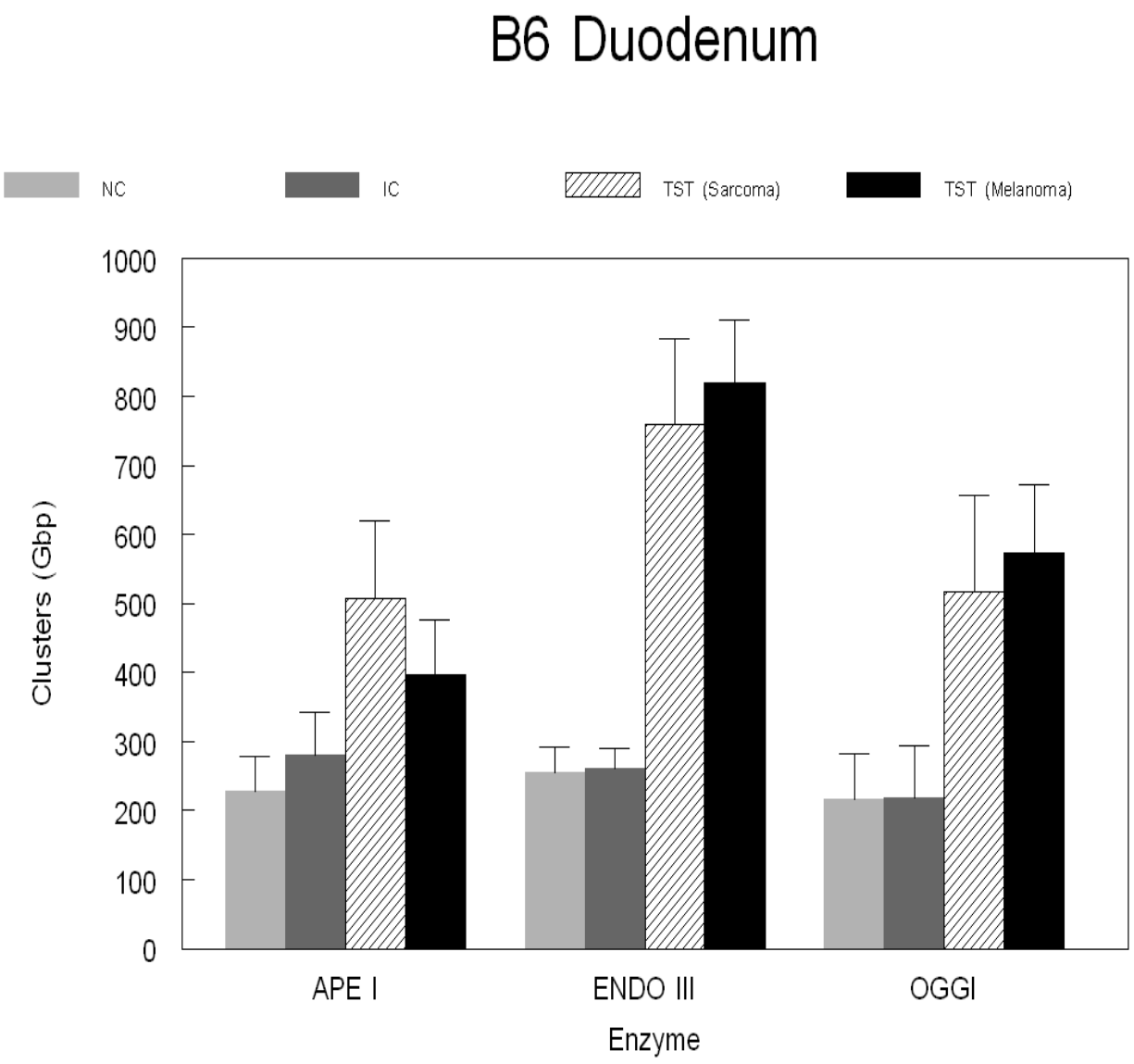

Figure 30: Cluster damage detected in duodenum tissue samples from the B6 experiment for the three different enzymes that were utilized. The Y axis corresponds to the number of clusters (Gbp) and the X axis corresponds to the three different enzymes.

Figure 31: Abasic Cluster Analysis – MCP-1 KO vs. B6

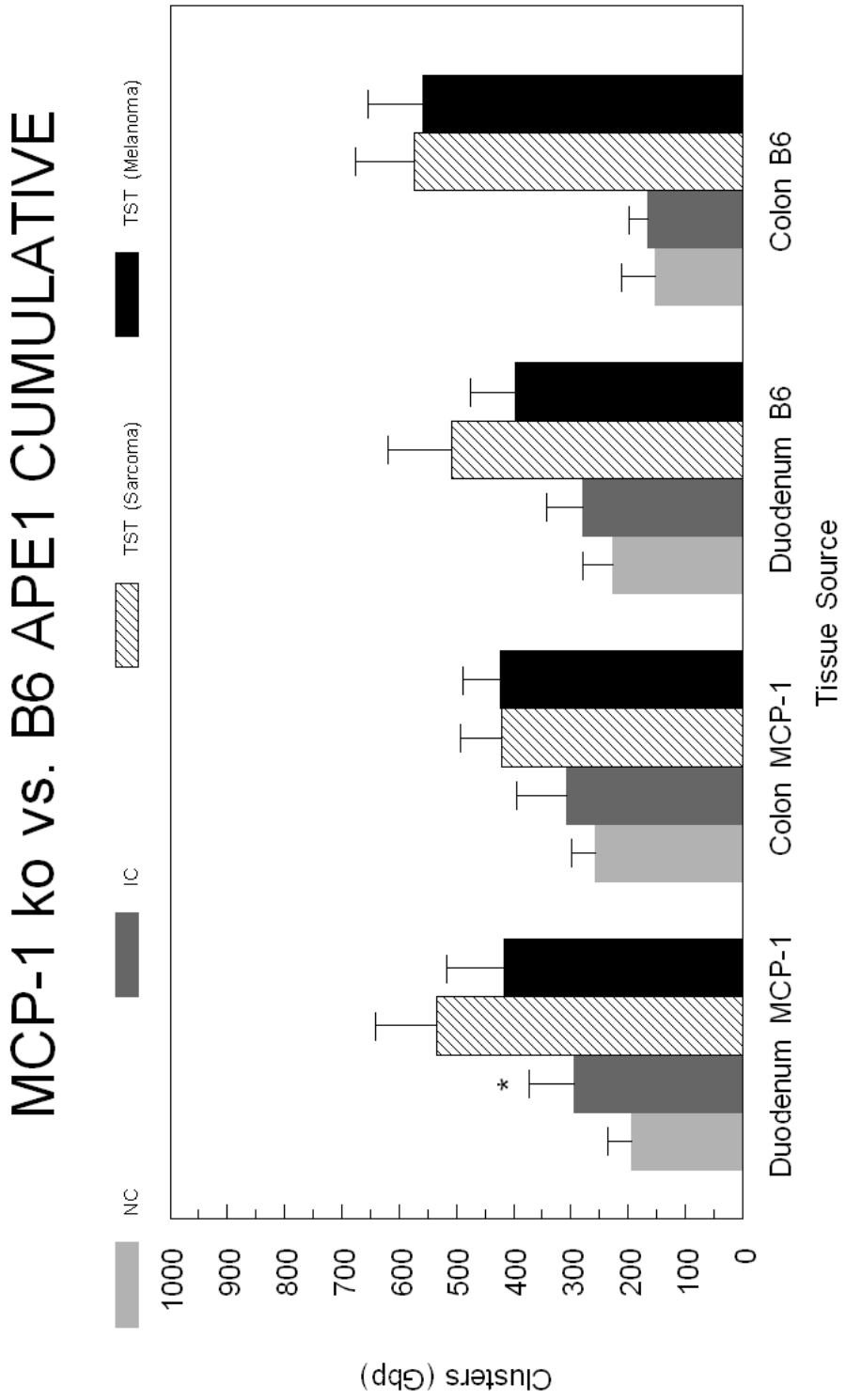

Figure 31: Abasic clusters that were detected from the MCP-1 ko vs. B6 Experiment. Significant cluster accumulation between MCP-1 ko inflammation control and MCP-1 ko TST (Melanoma) at $p<0.05$ is denoted by 'a'. Significant difference between MCP-1 ko inflammation control and MCP-1 ko TST (Sarcoma) is denoted by *. Significant difference between MCP-1 ko TST (Sarcoma) and B6 TST (Sarcoma) is denoted by **. Significant difference between MCP-1 ko TST (Melanoma) and B6 TST (Melanoma) is denoted by ***.

Figure 32: Oxypyrimidinic Cluster Analysis – MCP-1 KO vs. B6

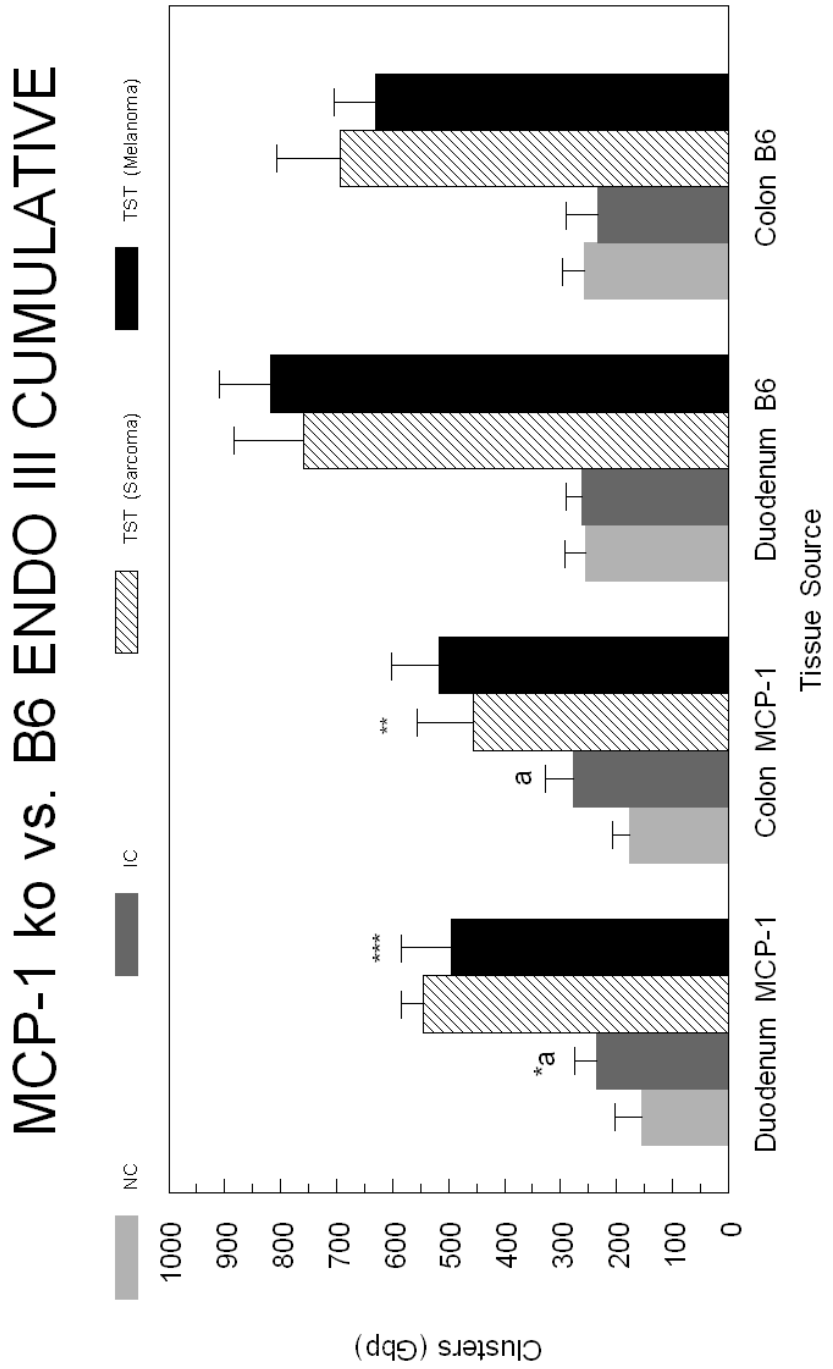

Figure 32: Oxypyrimidinic clusters that were detected from the MCP-1 ko vs. B6 Experiment. Significant cluster accumulation between MCP-1 ko inflammation control and MCP-1 ko TST (Melanoma) at $p<0.05$ is denoted by 'a'. Significant difference between MCP-1 ko inflammation control and MCP-1 ko TST (Sarcoma) is denoted by *. Significant difference between MCP-1 ko TST (Sarcoma) and B6 TST (Sarcoma) is denoted by **. Significant difference between MCP-1 ko TST (Melanoma) and B6 TST (Melanoma) is denoted by ***.

Figure 33: Oxypurinic Cluster Analysis – MCP-1 KO vs. B6

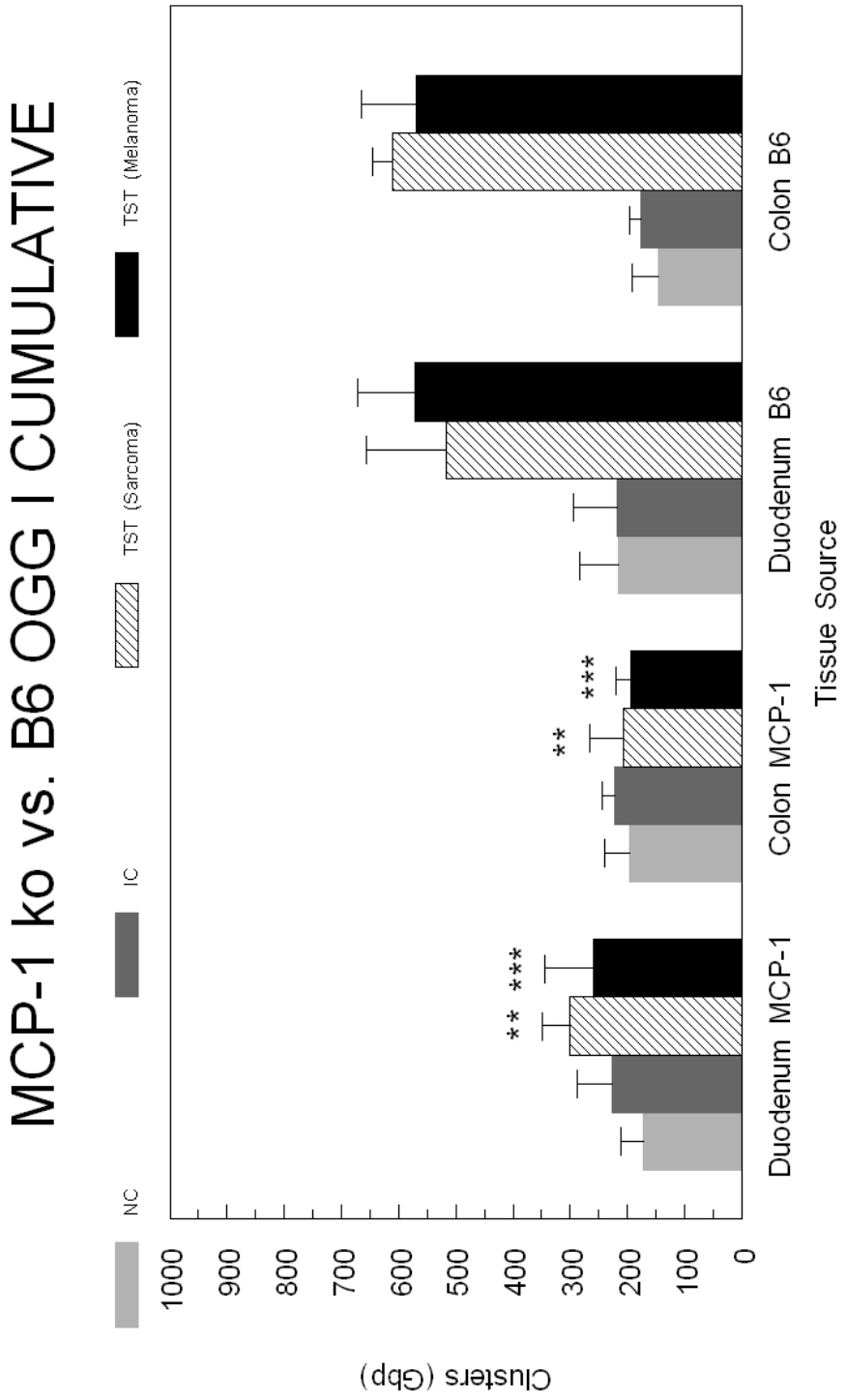

Figure 33: Oxypurinic clusters that were detected from the MCP-1 ko vs. B6 Experiment. Significant cluster accumulation between MCP-1 ko inflammation control and MCP-1 ko TST (Melanoma) at $p<0.05$ is denoted by 'a'. Significant difference between MCP-1 ko inflammation control and MCP-1 ko TST (Sarcoma) is denoted by *. Significant difference between MCP-1 ko TST (Sarcoma) and B6 TST (Sarcoma) is denoted by **. Significant difference between MCP-1 ko TST (Melanoma) and B6 TST (Melanoma) is denoted by ***.

Table 2: Lung Carcinoma Data

LUNG CARCINOMA				
Tissue:	**OVARY**			
Enzyme:		**APE Average Clusters (Gbp)**	**ENDO Average Clusters (Gbp)**	**OGG Average Clusters (Gbp)**
NC	**Average**	350.45	274.56	317.14
	Std. Dev	86.61	76.89	83.74
IC	**Average**	349.01	573.95	408.78
	Std. Dev	89.70	117.44	86.26
C+Tempol	**Average**	315.23	117.56	253.29
	Std. Dev	87.93	46.96	76.49
TST	**Average**	1076.04	1277.37	1091.11
	Std. Dev	243.60	113.08	193.26
TST+Tempol	**Average**	405.06	517.38	532.32
	Std. Dev	120.91	114.23	140.68
B6+TST	**Average**	1149.35	942.30	767.57
	Std. Dev	222.30	196.03	131.10
T-Test (IC vs. TST)	**p-value**	3.7E-06	2.8E-05	1.5E-05
T-Test (TST vs. TST+Tempol)	**p-value**	9.4E-06	6.4E-07	3.6E-04
T-Test (TST vs. B6+TST)	**p-value**	3.0E-01	7.7E-01	1.5E-01

Raw data obtained from lung carcinoma experiment. Averages are from three replicate sets.

Student paired T-test was performed as paired analysis; $p<0.05$.

Tissue:	SPLEEN			
Enzyme:		APE Average Clusters (Gbp)	ENDO Average Clusters (Gbp)	OGG Average Clusters (Gbp)
NC	Average	234.65	226.39	196.15
	Std. Dev	79.67	75.39	59.77
IC	Average	381.28	497.81	541.61
	Std. Dev	139.58	88.04	148.51
C+Tempol	Average	290.09	232.13	380.79
	Std. Dev	98.25	86.82	96.79
TST	Average	965.57	1100.17	883.29
	Std. Dev	213.95	88.72	180.10
TST+Tempol	Average	455.56	485.61	350.37
	Std. Dev	139.14	143.09	89.16
B6+TST	Average	1204.95	917.33	1175.87
	Std. Dev	212.65	218.20	181.67
T-Test (IC vs. TST)	p-value	9.4E-05	3.0E-04	3.9E-03
T-Test (TST vs. TST+Tempol)	p-value	4.8E-04	2.4E-06	3.7E-05
T-Test (TST vs. B6+TST)	p-value	5.1E-02	1.1E-01	1.8E-01

Raw data obtained from lung carcinoma experiment. Averages are from three replicate sets.

Student paired T-test was performed as paired analysis; $p<0.05$.

Tissue:	DUODENUM			
Enzyme:		APE Average Clusters (Gbp)	ENDO Average Clusters (Gbp)	OGG Average Clusters (Gbp)
NC	Average	297.17	245.44	396.16
	Std. Dev	121.55	81.13	111.62
IC	Average	431.96	230.58	467.72
	Std. Dev	139.07	69.61	108.89
C+Tempol	Average	248.41	253.21	376.01
	Std. Dev	91.16	80.90	93.88
TST	Average	921.73	1331.18	1232.05
	Std. Dev	243.00	195.25	204.02
TST+Tempol	Average	441.87	758.66	578.74
	Std. Dev	130.13	167.80	159.73
B6+TST	Average	1235.08	1249.94	834.60
	Std. Dev	273.89	208.47	127.99
T-Test (IC vs. TST)	p-value	4.5E-03	3.4E-06	1.7E-05
T-Test (TST vs. TST+Tempol)	p-value	1.1E-02	2.0E-03	3.1E-05
T-Test (TST vs. B6+TST)	p-value	5.9E-02	6.8E-01	1.6E-01

Raw data obtained from lung carcinoma experiment. Averages are from three replicate sets.

Student paired T-test was performed as paired analysis; $p<0.05$.

Tissue:	COLON			
Enzyme:		APE Average Clusters (Gbp)	ENDO Average Clusters (Gbp)	OGG Average Clusters (Gbp)
NC	Average	250.48	166.73	215.85
	Std. Dev	84.72	55.11	60.63
IC	Average	434.33	371.17	533.77
	Std. Dev	152.77	94.83	108.53
C+Tempol	Average	257.53	234.99	255.62
	Std. Dev	77.27	88.70	85.19
TST	Average	1063.02	1161.22	981.95
	Std. Dev	247.30	187.03	146.86
TST+Tempol	Average	429.90	574.85	478.96
	Std. Dev	121.29	140.53	114.59
B6+TST	Average	1010.25	928.44	685.16
	Std. Dev	213.95	193.88	103.63
T-Test (IC vs. TST)	p-value	2.9E-03	1.5E-03	3.0E-02
T-Test (TST vs. TST+Tempol)	p-value	7.6E-04	1.7E-02	1.9E-02
T-Test (TST vs. B6+TST)	p-value	6.5E-01	2.9E-01	2.3E-01

Raw data obtained from lung carcinoma experiment. Averages are from three replicate sets.

Student paired T-test was performed as paired analysis; $p<0.05$.

Tissue:	STOMACH			
Enzyme:		APE Average Clusters (Gbp)	ENDO Average Clusters (Gbp)	OGG Average Clusters (Gbp)
NC	Average	365.94	280.02	280.37
	Std. Dev	83.76	99.89	90.37
IC	Average	402.04	385.10	458.40
	Std. Dev	101.19	113.18	94.26
C+Tempol	Average	393.59	536.72	386.61
	Std. Dev	117.54	159.58	116.51
TST	Average	1209.39	1483.56	1074.38
	Std. Dev	271.09	200.14	180.59
TST+Tempol	Average	397.23	663.42	553.55
	Std. Dev	98.38	113.16	99.99
B6+TST	Average	1516.00	1016.64	1376.48
	Std. Dev	298.79	177.73	297.15
T-Test (IC vs. TST)	p-value	7.0E-04	6.7E-07	1.5E-04
T-Test (TST vs. TST+Tempol)	p-value	1.5E-04	1.0E-06	1.4E-04
T-Test (TST vs. B6+TST)	p-value	1.4E-01	4.8E-01	7.7E-02

Raw data obtained from lung carcinoma experiment. Averages are from three replicate sets.

Student paired T-test was performed as paired analysis; $p<0.05$.

Tissue:	RECTUM			
Enzyme:		APE Average Clusters (Gbp)	ENDO Average Clusters (Gbp)	OGG Average Clusters (Gbp)
NC	Average	159.96	161.18	284.67
	Std. Dev	48.65	72.90	86.73
IC	Average	386.01	494.42	345.13
	Std. Dev	83.70	103.43	97.48
C+Tempol	Average	180.63	271.67	140.43
	Std. Dev	62.52	76.35	58.03
TST	Average	1075.70	951.26	946.52
	Std. Dev	212.46	147.14	218.52
TST+Tempol	Average	372.99	582.61	391.18
	Std. Dev	88.86	98.84	140.15
B6+TST	Average	1218.87	1109.07	965.91
	Std. Dev	220.65	153.46	184.20
T-Test (IC vs. TST)	p-value	3.2E-05	1.0E-03	1.1E-05
T-Test (TST vs. TST+Tempol)	p-value	1.9E-05	8.3E-03	5.4E-06
T-Test (TST vs. B6+TST)	p-value	3.0E-01	1.9E-01	9.4E-01

Raw data obtained from lung carcinoma experiment. Averages are from three replicate sets.

Student paired T-test was performed as paired analysis; $p<0.05$.

Tissue:	SKIN DISTAL			
Enzyme:		APE Average Clusters (Gbp)	ENDO Average Clusters (Gbp)	OGG Average Clusters (Gbp)
NC	Average	438.82	436.41	319.50
	Std. Dev	110.60	78.56	83.20
IC	Average	282.77	358.34	138.23
	Std. Dev	159.29	122.53	99.94
C+Tempol	Average	384.10	414.92	565.26
	Std. Dev	94.78	139.72	65.37
TST	Average	908.48	1209.63	1008.00
	Std. Dev	77.53	168.49	161.13
TST+Tempol	Average	454.16	578.00	475.53
	Std. Dev	98.54	121.38	99.05
B6+TST	Average	1386.87	818.21	723.55
	Std. Dev	136.90	139.98	119.38
T-Test (IC vs. TST)	p-value	2.5E-03	5.7E-03	1.2E-03
T-Test (TST vs. TST+Tempol)	p-value	3.4E-03	2.3E-04	3.9E-03
T-Test (TST vs. B6+TST)	p-value	3.0E-01	5.9E-02	9.0E-02

Raw data obtained from lung carcinoma experiment. Averages are from three replicate sets.

Student paired T-test was performed as paired analysis; $p<0.05$.

Tissue:	SKIN CERVICAL			
Enzyme:		APE Average Clusters (Gbp)	ENDO Average Clusters (Gbp)	OGG Average Clusters (Gbp)
NC	Average	342.05	244.32	252.09
	Std. Dev	116.33	83.97	62.88
IC	Average	335.70	300.54	318.43
	Std. Dev	102.71	78.78	79.58
C+Tempol	Average	287.24	213.05	323.37
	Std. Dev	62.30	94.11	92.18
TST	Average	1508.66	1428.47	1217.42
	Std. Dev	276.92	234.03	116.74
TST+Tempol	Average	444.45	453.18	579.95
	Std. Dev	113.06	118.17	122.46
B6+TST	Average	1312.92	1173.17	1211.05
	Std. Dev	216.75	165.88	153.18
T-Test (IC vs. TST)	p-value	4.6E-05	1.4E-06	4.6E-08
T-Test (TST vs. TST+Tempol)	p-value	5.8E-05	1.2E-05	3.4E-05
T-Test (TST vs. B6+TST)	p-value	2.1E-01	2.9E-01	6.5E-01

Raw data obtained from lung carcinoma experiment. Averages are from three replicate sets.

Student paired T-test was performed as paired analysis; $p<0.05$.

Tissue:	TUMOR			
Enzyme:		APE Average Clusters (Gbp)	ENDO Average Clusters (Gbp)	OGG Average Clusters (Gbp)
NC	Average	438.82	436.41	319.50
	Std. Dev	110.60	78.56	83.20
IC	Average	259.26	385.34	138.23
	Std. Dev	62.73	122.53	44.70
C+Tempol	Average	384.10	414.92	565.26
	Std. Dev	94.87	139.72	65.37
TST	Average	876.84	1203.88	1229.35
	Std. Dev	170.73	154.40	186.35
TST+Tempol	Average	538.27	601.64	467.88
	Std. Dev	112.45	129.23	99.70
B6+TST	Average	1224.26	1357.29	1793.98
	Std. Dev	212.15	145.14	106.08
T-Test (IC vs. TST)	p-value	2.1E-03	1.6E-03	6.3E-04
T-Test (TST vs. TST+Tempol)	p-value	7.4E-03	2.6E-03	1.5E-03
T-Test (TST vs. B6+TST)	p-value	1.9E-01	3.0E-01	6.6E-03

Raw data obtained from lung carcinoma experiment. Averages are from three replicate sets.

Student paired T-test was performed as paired analysis; $p<0.05$.

Table 3: MCP-1 / B6 Data

MCP-1 KO				
Tissue:	**DUODENUM**			
Enzyme:		**APE Average Clusters (Gbp)**	**ENDO Average Clusters (Gbp)**	**OGG Average Clusters (Gbp)**
NC	**Average**	193.40	154.08	172.09
	Std. Dev	43.08	49.15	39.40
IC	**Average**	295.28	236.47	227.84
	Std. Dev	77.24	38.86	59.34
TST+Melanoma	**Average**	416.83	494.73	260.24
	Std. Dev	100.36	90.22	84.49
TST+Sarcoma	**Average**	534.43	544.77	300.05
	Std. Dev	107.09	40.44	48.14
T-Test (IC vs. TST+Melanoma)	**p-value**	3.5E-01	1.8E-02	8.2E-01
T-Test (IC vs. TST+Sarcoma)	**p-value**	1.1E-01	2.1E-02	2.5E-01
T-Test (MCP-1 vs. B6 (Melanoma))	**p-value**	5.8E-02	8.2E-02	1.7E-02
T-Test (MCP-1 vs. B6 (Sarcoma))	**p-value**	1.1E-02	6.2E-02	8.6E-02

Raw data obtained from MCP-1 ko / B6 experiment. Averages are from three replicate sets.

Student paired T-test was performed as paired analysis; $p<0.05$.

MCP-1 KO				
Tissue:	**COLON**			
Enzyme:		**APE Average Clusters (Gbp)**	**ENDO Average Clusters (Gbp)**	**OGG Average Clusters (Gbp)**
NC	**Average**	257.30	176.60	196.61
	Std. Dev	42.50	30.16	42.74
IC	**Average**	307.05	277.77	221.53
	Std. Dev	88.19	49.34	22.04
TST+Melanoma	**Average**	422.96	517.77	193.70
	Std. Dev	65.46	83.72	26.94
TST+Sarcoma	**Average**	420.33	455.52	207.05
	Std. Dev	71.54	100.36	58.05
T-Test (IC vs. TST+Melanoma)	**p-value**	1.4E-01	7.1E-03	6.4E-01
T-Test (IC vs. TST+Sarcoma)	**p-value**	1.8E-01	8.5E-02	4.3E-01
T-Test (MCP-1 vs. B6 (Melanoma))	**p-value**	1.0E-01	3.5E-01	1.0E-02
T-Test (MCP-1 vs. B6 (Sarcoma))	**p-value**	5.3E-02	4.9E-03	1.4E-02

Raw data obtained from MCP-1 ko / B6 experiment. Averages are from three replicate sets.

Student paired T-test was performed as paired analysis; $p<0.05$.

B6				
Tissue:	**DUODENUM**			
Enzyme:		**APE Average Clusters (Gbp)**	**ENDO Average Clusters (Gbp)**	**OGG Average Clusters (Gbp)**
NC	**Average**	227.33	254.55	216.08
	Std. Dev	50.83	36.88	66.89
IC	**Average**	279.99	262.00	217.82
	Std. Dev	61.83	27.86	77.08
TST+Melanoma	**Average**	396.11	818.88	572.22
	Std. Dev	79.60	91.02	100.05
TST+Sarcoma	**Average**	507.25	758.26	517.81
	Std. Dev	111.70	125.89	138.12

Raw data obtained from MCP-1 ko / B6 experiment. Averages are from three replicate sets.

Student paired T-test was performed as paired analysis; $p<0.05$.

B6				
Tissue:	**COLON**			
Enzyme:		**APE Average Clusters (Gbp)**	**ENDO Average Clusters (Gbp)**	**OGG Average Clusters (Gbp)**
NC	**Average**	153.58	256.92	146.88
	Std. Dev	57.90	40.05	44.87
IC	**Average**	166.03	233.68	177.24
	Std. Dev	33.51	56.55	18.34
TST+Melanoma	**Average**	558.95	630.88	568.95
	Std. Dev	96.38	73.95	95.62
TST+Sarcoma	**Average**	574.08	693.09	609.88
	Std. Dev	102.37	113.11	34.90

Raw data obtained from MCP-1 ko / B6 experiment. Averages are from three replicate sets.

Student paired T-test was performed as paired analysis; $p<0.05$.

CHAPTER 6: DISCUSSION

Cancer continues to be one of the leading causes of death in the United States. Like many diseases, with earlier detection there is improved prognosis and more efficient treatment. In this study, three tumors were studied, lung carcinoma, melanoma and sarcoma, and subjected to various treatments. Analysis was performed to assess the amount of DNA damage, more specifically, the amount of OCDL formation. With different cohorts, we were able to elucidate sources of OCDL formation.

For the lung carcinoma experiments, a comparison between the inflammation control and normal control mice tissues were made. There was an overall insignificant elevation in OCDL formation in the tissues for the mice that have been subjected to Freund's adjuvant. As mentioned above, a trend is noted, but there is no significant difference between the two cohorts. This suggests that basal inflammation increases OCDL levels, but is not the only biological mechanism that induces OCDL formation.

A comparison was made between the inflammation control mice, the PBS control mice and the tumor bearing mice. In the tissues for all three enzymes, there is an increase in OCDL formation when the tumor is present. As opposed to my second hypothesis, regardless of the tissues being distal or proximal to the tumor, there is an increase in OCDL. This can be explained by the general increase in oxidative stress when the tumor is present. This effect is mediated by different cytokines, inflammation, ROS and RNS transmitted by the bystander/distal effect. The bystander/distal effect that was observed portrays the induction of DNA damage to tissues that are both proximal and distal to the site of tumor injection.

The next comparison for the lung carcinoma experiment was with the addition of the antioxidant Tempol. The superoxide dismutase scavenges superoxide anions and neutralizes

them, thereby decreasing the level of intracellular oxidative stress. When comparing the mice plus the antioxidant Tempol to mice bearing lung carcinoma we see a significant decrease in OCDL formation. The significance is seen with the majority of the tissues for all three enzymes. From this, it can be concluded that a decrease in oxidative stress results into a decreased accumulation of OCDLs.

A final comparison for the lung carcinoma experiment looked at nude mice bearing the tumor vs. B6 tumor bearing mice. The nude mice lack a thymus. Because of this, there is no T-cell mediated response to tumors being present. Although there is no T-cell response, a cytokine analysis was performed on the nude mice. The presence of numerous cytokines was observed, but at lower levels when compared to B6 mice with the tumor where there was an increase ~3.5 fold. When nude mice bearing a tumor were compared to B6 mice bearing a tumor, the OCDL formation showed no significant difference between the two cohorts. There was no trend that was established. This suggests that while the adaptive immunity may play a role in OCDL formation, a more profound role is seen with biological responses such as, cytokines, inflammation and innate immune, in the induction of OCDL formation.

The rate of proliferation plays a significant role in the susceptibility of DNA damage and ROS productivity. Because of this, it was expected that the tissues with the highest rate of proliferation, such as the tissues from the GI tract, would exhibit the greatest amount of OCDL induction. This was not always verified. In several cases, such as with the addition of APE1, the ovary and lung exhibit an equivalent frequency of OCDL formation.

In a cytokine analysis performed by Redon et al, monocyte chemoattractant protein-1 (MCP-1) was observed to be up-regulated in the presence of tumors. MCP-1 functions as a signal for the recruitment of monocytes to a site of damage or injury. An increase in oxidative stress is

associated with the recruitment of monocytes and immunological response. Therefore, it is expected that with MCP-1 knocked out, there will be a decrease in overall oxidative stress and lower OCDL formation.

MCP-1 functions as a stimulant for TGF-β. TGF-β is a protein in the body that assists with the regulation of cell proliferation. With MCP-1 being knocked out, it is expected that cellular proliferation will be reduced.

A comparison was performed between inflammation control MCP-1 ko mice with MCP-1 ko mice bearing tumors. Two tissues were tested, the duodenum and colon. Interestingly, for the colon, both abasic and oxypurine enzymes detected no statistical significant difference between the inflammation control and the melanoma bearing mice for MCP-1 ko in the mice. The mice bearing sarcoma and MCP-1 ko, all three enzymes did not detect a statistical difference when compared to MCP-1 ko inflammation control. The duodenum displayed similar results. Both abasic (APE1) and oxypurine (OGG1) enzymes detected no statistical difference between the melanoma bearing mice and the inflammation control for the MCP-1 ko mice. Only oxypurine enzyme detection displayed no statistical difference between sarcoma bearing mice and the inflammation control for the MCP-1 ko mice.

A final comparison was composed assessing the differences between tumor bearing mice with MCP-1 ko and B6 tumor bearing mice. For the enzyme that detects oxypurines (OGG1), both the duodenum and colon show a significant decrease in OCDL formation for the tumor bearing mice with MCP-1 ko versus B6 tumor bearing mice. It is also seen for detection of oxypyrimidines, the colon displays a significant difference for the MCP-1 ko sarcoma bearing mice as compared to the B6 mice with the corresponding tumor. A significant difference is also

established for the duodenum tissue between the MCP-1 ko melanoma bearing mice when compared to the B6 mice bearing the corresponding tumor.

The induction of oxidative damage was seen in tissues both proximal and distal to the tumor mass. This indicates the existence of one or more communication pathways being present between tissues. It has been demonstrated from previous studies that inflammation is a source of the bystander effect. Cytokines and intercellular communication have also been implemented as a source of this effect. This study shows for the first time that the manifestation of OCDLs in distant tissues is strongly mediated by the cytokine MCP-1.

In a previous study performed by Redon *et al*, γ-H2AX analysis was performed to assess the DNA double stranded break damage in association with the presence of a tumor. Phosphorylated histone is utilized to detect the presence of DNA damage. It was seen that for the tissues that MCP-1 was knocked out, there was a decrease in double stranded breaks. Interestingly, this corresponds to the results that were obtained from the OCDL analysis that we performed. With the removal of the MCP-1 gene, there was a decrease in OCDL damage. This signifies MCP-1 as having a key role in the induction of DNA damage.

With the findings from Redon *et al* and the findings from this experiment, there is a demonstration that the presence of tumors may induce an increase in the level of inflammation and damage that is sufficient to induce DNA damage in tissues both proximal and distal to the tumor. Furthermore, from this experiment, it can be seen with chronic inflammation, damage to DNA can arise, including an elevated risk for cancer formation. Induction and detection of OCDL formation along with further comprehension of the bystander/distal effect and the associated DNA damages will have great impacts in the clinical aspects of oncology prognosis and detection. It is hopeful to one day implement tissue biopsies for OCDL screening which in

turn will act as a biomarker for tumor presence and allow earlier prognosis. With earlier prognosis, treatments will be more effective ultimately leading to greater probability of remission.

It is essential to expand this study and examine different tissues to truly grasp the effects of the bystander/distal phenomenon. Currently, two other carcinomas are be analyzed for OCDL formation along with broader tissue samples, such as the brain and kidneys. These studies will utilize B6 mice as their test cohorts along with the addition of the antioxidant Tempol.

REFERENCES

Ames, B. N., M. K. Shigenaga, et al. (1993). "Oxidants, antioxidants, and the degenerative diseases of aging." Proc Natl Acad Sci U S A 90(17): 7915-22.

Averbeck, D., K. Polasa, et al. (1993). "Photobiological activities of 1,6-dioxapyrene in pro- and eukaryotic cells." Mutat Res 287(2): 165-79.

Bennett, P. V., N. S. Cintron, et al. (2004). "Are endogenous clustered DNA damages induced in human cells?" Free Radic Biol Med 37(4): 488-99.

Bohr, V. A. (2002). "DNA damage and its processing. relation to human disease." J Inherit Metab Dis 25(3): 215-22.

Braunersreuther, V., F. Mach, et al. (2007). "The specific role of chemokines in atherosclerosis." Thromb Haemost 97(5): 714-21.

Cadet, J., S. Bellon, et al. (2004). "Radiation-induced DNA damage: formation, measurement, and biochemical features." J Environ Pathol Toxicol Oncol 23(1): 33-43.

Chatterjee, P. K., S. Cuzzocrea, et al. (2000). "Tempol, a membrane-permeable radical scavenger, reduces oxidant stress-mediated renal dysfunction and injury in the rat." Kidney Int 58(2): 658-73.

Chaudhry, M. A. and M. Weinfeld (1997). "Reactivity of human apurinic/apyrimidinic endonuclease and Escherichia coli exonuclease III with bistranded abasic sites in DNA." J Biol Chem 272(25): 15650-5.

Dewald, O., P. Zymek, et al. (2005). "CCL2/Monocyte Chemoattractant Protein-1 regulates inflammatory responses critical to healing myocardial infarcts." Circ Res 96(8): 881-9.

Dickey, J. S., B. J. Baird, et al. (2009). "Intercellular communication of cellular stress monitored by gamma-H2AX induction." Carcinogenesis 30(10): 1686-95.

Dizdaroglu, M., P. Jaruga, et al. (2002). "Free radical-induced damage to DNA: mechanisms and measurement." Free Radic Biol Med 32(11): 1102-15.

Epe, B. (2002). "Role of endogenous oxidative DNA damage in carcinogenesis: what can we learn from repair-deficient mice?" Biol Chem 383(3-4): 467-75.

Georgakilas, A. G. (2008). "Processing of DNA damage clusters in human cells: current status of knowledge." Mol Biosyst 4(1): 30-5.

Gollapalle, E., R. Wang, et al. (2007). "Detection of oxidative clustered DNA lesions in X-irradiated mouse skin tissues and human MCF-7 breast cancer cells." Radiat Res 167(2): 207-16.

Gros, L., M. K. Saparbaev, et al. (2002). "Enzymology of the repair of free radicals-induced DNA damage." Oncogene 21(58): 8905-25.

Hada, M. and A. G. Georgakilas (2008). "Formation of clustered DNA damage after high-LET irradiation: a review." J Radiat Res (Tokyo) 49(3): 203-10.

Little, J. B., E. I. Azzam, et al. (2002). "Bystander effects: intercellular transmission of radiation damage signals." Radiat Prot Dosimetry 99(1-4): 159-62.

Nowsheen, S., R. L. Wukovich, et al. (2009). "Accumulation of oxidatively induced clustered DNA lesions in human tumor tissues." Mutat Res 674(1-2): 131-6.

Popivanova, B. K., F. I. Kostadinova, et al. (2009). "Blockade of a chemokine, CCL2, reduces chronic colitis-associated carcinogenesis in mice." Cancer Res 69(19): 7884-92.

Prise, K. M., M. Folkard, et al. (2003). "A review of the bystander effect and its implications for low-dose exposure." Radiat Prot Dosimetry 104(4): 347-55.

Prise, K. M. and J. M. O'Sullivan (2009). "Radiation-induced bystander signalling in cancer therapy." Nat Rev Cancer 9(5): 351-60.

Redon, C. E., J. S. Dickey, et al. "Tumors induce complex DNA damage in distant proliferative tissues in vivo." Proc Natl Acad Sci U S A.

Sebald, W., J. Nickel, et al. "Molecular basis of cytokine signalling--theme and variations." Febs J 277(1): 106-18.

Sedelnikova, O. A., A. Nakamura, et al. (2007). "DNA double-strand breaks form in bystander cells after microbeam irradiation of three-dimensional human tissue models." Cancer Res 67(9): 4295-302.

Sokolov, M. V., L. B. Smilenov, et al. (2005). "Ionizing radiation induces DNA double-strand breaks in bystander primary human fibroblasts." Oncogene 24(49): 7257-65.

Sutherland, B. M., P. V. Bennett, et al. (2000). "Clustered damages and total lesions induced in DNA by ionizing radiation: oxidized bases and strand breaks." Biochemistry 39(27): 8026-31.

Sutherland, B. M., A. G. Georgakilas, et al. (2003). "Quantifying clustered DNA damage induction and repair by gel electrophoresis, electronic imaging and number average length analysis." Mutat Res 531(1-2): 93-107.

Vilenchik, M. M. and A. G. Knudson (2003). "Endogenous DNA double-strand breaks: production, fidelity of repair, and induction of cancer." Proc Natl Acad Sci U S A 100(22): 12871-6.

APPENDIX: SAFETY COMPLIANCE FORMS

Environmental Health and Safety
East Carolina University
210 East Fourth Street – Greenville, NC 27858-4353
252-328-6166 office ~ **252-737-1458** fax
www.ecu.edu/oehs

Emergency Response
Environmental Management
Industrial Hygiene
Occupational Safety
Workers' Compensation

To: Thomas Kryston

From: Kelly Shook, Health Sciences Coordinator
Office of Environmental Health and Safety

Date: November 2, 2010

Subject: Chemical Hygiene/Laboratory Safety Training

Dear Mr. Kryston,

This letter is to serve as documentation that you have successfully completed the Chemical Hygiene/Laboratory Safety training as required by the Office of Environmental Health and Safety. Your attendance is on file with our office as well as on OneStop.

This training was initiated upon revision of the East Carolina University Chemical Hygiene Plan in September 2010. Topics included standard safety procedures applicable to all ECU laboratories, as well as responsibilities, chemical management and medical consultation. This training is considered current until the Fall 2013 revision and updated training program.

Please contact me with any questions or concerns.

Sincerely,

Kelly E Shook

Kelly E. Shook, MSEH, AOES
Health Sciences Coordinator
Office of Environmental Health and Safety
East Carolina University